Available online at www.sciencedirect.com
ScienceDirect
Comput. Methods Appl. Mech. Engrg. 415 (2023) 116281
Computer methods in applied mechanics and engineering
www.elsevier.com/locate/cma

Univariate Gauss quadrature for structural modelling of tissues and materials with distributed fibres

Ben R. Britt*, Alexander E. Ehret*

Empa, Swiss Federal Laboratories for Materials Science and Technology, Überlandstrasse 129, CH-8600 Dübendorf, Switzerland
ETH Zurich, Institute for Mechanical Systems, Leonhardstrasse 21, CH-8092 Zürich, Switzerland

Received 8 May 2023; received in revised form 11 July 2023; accepted 11 July 2023
Available online 2 August 2023

Abstract

This work presents a method for computing the averaged free energy and constitutive relations in hyperelastic material models with distributed fibres, as they apply to soft fibre-reinforced materials and biological tissues. While these models are currently implemented through either spherical cubature of the fibre free energy or its Taylor series, we here propose a new method based on a univariate Gauss quadrature rule with integration points and weights informed by the statistical moments of the distribution of fibre stretch. As an intrinsic property, the new approach separates the integration of the fibre constitutive law from the integration of the orientation distribution, the latter leading to structural tensors of even order. Provided the latter $2n-1$ tensors are computed accurately up to tensorial order $2(2n-1)$, the method integrates exactly any polynomial of order $2n-1$ that agrees with the fibre law at the n integration points. After formally introducing the quadrature method for generally non-affine fibre deformations and arbitrary order, we focus on the important special case of affine fibre kinematics and discuss the rules with $n \leq 3$ integration points, for which the corresponding positions and weights are determined analytically. At a computational cost comparable to the existing approaches, the new method does not require the fibre law to be analytic and can thus robustly deal with piece-wise definitions of the fibre energy, in contrast to Taylor-series approaches, and it does not induce additional anisotropy as it can occur with spherical cubature rules. The 3-point rule is further investigated and illustrated in numerical examples relating to soft collagenous tissues based on a Fortran implementation of the method suitable for use in finite element analyses.

Keywords: Moment-based quadrature; Statistical moments; Stretch distribution; Multiscale modelling; Generalised structural tensors; Anisotropy

1. Introduction

The efficient computation of averaged non-linear properties of materials that feature fibre network microstructures or that are reinforced by statistically distributed fibres represents an essential steps in various fields of mechanics. A prominent example is the biomechanics of soft collagenous tissues, which is at the basis of various analyses that help understanding the mechanical functioning of the body in the physiological state, allow studying the development of

* Corresponding authors at: Empa, Swiss Federal Laboratories for Materials Science and Technology, Überlandstrasse 129, CH-8600 Dübendorf, Switzerland.
E-mail addresses: ben-rudolf.britt@empa.ch (B.R. Britt), alexander.ehret@empa.ch (A.E. Ehret).

https://doi.org/10.1016/j.cma.2023.116281

pathological conditions induced or accompanied by changes of the mechanical environment, and that finally support the development of biomedical materials and devices.

Integrating basic information on tissue microstructure into constitutive models that represent the mechanical behaviour of the material at macroscopic length scale has been an objective pursued by the biomechanics community for a long time, and has led to various approaches, both tissue-specific and general ones. One of the most popular strategies is the method known as structural modelling [1], which is typically associated with the pioneering work of Y. Lanir [2]. Briefly, the ensemble response of fibres, each associated with an alignment direction in space, is obtained by an average of a single fibre's response over the set of all possible directions, potentially weighted by an orientation probability density function in case the orientation distribution is not uniform. The directional 'space' is conveniently represented by the unit sphere in 2 or 3 dimensions for planar and bulk tissues, respectively, so that the averaging operation results in a spherical integral.

Spherical integration has become a 'canonical' strategy to address the averaging problem, not only in biomechanics but also in various other fields of mechanics. The generally highly non-linear fibre properties potentially multiplied by likewise non-linear orientation distributions usually forbid an analytic solution of the integrals and call for numerical methods. The two most common approaches in this regard concern numerical cubature on the sphere [3], and analytic approximations based on a Taylor-series expansion of the fibre related properties [see e.g. the review in 4].

Both these approaches require the existence of a relation between the response of a single fibre with given initial orientation and the macroscopic state of deformation. Although it has frequently been shown that such a deterministic relation between fibre orientation and stretch is generally lacking in non-affine fibre networks [5–8], several models were proposed to link fibre orientation and stretch [e.g. 9–13], and most prominent is the assumption of affine deformations.

In the affine case, the fibre square stretch is a quadratic spherical polynomial linear in the components of the macroscopic right Cauchy–Green tensor. Hence, if the fibre response is defined in terms of an analytical function of its square stretch, the integrand may represent an infinite series of analytically integrable terms, at least in the case of uniform orientation distributions. If the orientation distribution is non-uniform, i.e. the network anisotropic, it additionally depends on the form of the latter, whether the product of fibre energy and distribution density to be integrated maintains this beneficial property. Therefore both methods, spherical cubature and Taylor-series-based analytical approaches, can be shown to be exact in the special cases where the series is finite and the integrand represents a spherical polynomial of some degree n. However, the observed non-linear properties of collagen fibre bundles are often expressed in terms of non-polynomial functions; asymptotes in the constitutive fibre law are sometimes used to reflect limiting strains [14,15]; fibre switches [16] are considered to reflect tension-compression asymmetry of slender fibres; eventually highly non-linear orientation distributions are typically employed to reflect the dispersion of the collagen fibres within the tissue. All these characteristics derogate a potentially polynomial character of the integrand.

As a consequence both methods, spherical cubature and Taylor-series-based analytical approaches generally represent approximations, whereby the quality largely scales with the computational cost. In the Taylor-series-based approach, quality and cost depend on the number of considered terms before the series is truncated. For spherical cubature, they generally increase with the number of integration points on the sphere, each associated with an evaluation of the integrand. In addition, both methods come with their own special weakness, that tends to vanish only slowly when increasing the computational efforts. Spherical cubature is known to impair the intended material symmetry of the model [17], while the analytic approach has strong limitations dealing with fibre switches that lead to discontinuities in the derivatives of the integrand [4].

In recent work [4,18], we have shown that the averaged free energy of networks of elastic fibres can be formulated in an alternative way in terms of the distribution of fibre stretch, or suitable functions of the latter. The average free energy density of the network, which is a scalar multiple of the expectation of the fibre free energy density, results as a one-dimensional integral on the positive reals $\mathbb{R}_{>0}$ [18]. In the affine case it lives on the support bounded by the minimum and maximum macroscopic principal stretch. In general, a wealth of numerical quadrature methods exists to approximately solve such integrals, and here we propose the use of Gauss-quadrature to address this task. We exemplify how the moment-based Gauss quadrature [19] can be used to integrate structural models in biomechanics [20–22], that take account of statistically distributed fibre orientations. We show that this method represents a robust technique that can actually compete with the existing approaches. Given that the thus obtained approximations are both free of induced anisotropy and robust against piecewise-defined, non-smooth fibre strain-energies, the proposed approach may even present the method of choice for applications in soft tissue biomechanics.

2. Preliminaries

2.1. Kinematics and stress in hyperelastic materials

The deformation of a material body is described by the mapping $\boldsymbol{\varphi} : \mathcal{B}_0 \to \mathcal{B}_t$, $\boldsymbol{X} \mapsto \boldsymbol{x}$, taking a material point from its reference position $\boldsymbol{X}$ in the referential configuration $\mathcal{B}_0$ to its current position $\boldsymbol{x}$ in the current configuration $\mathcal{B}_t$. The corresponding deformation gradient $\mathbf{F} = \partial\boldsymbol{\varphi}/\partial\boldsymbol{X}$ with determinant $J = \det\mathbf{F} > 0$ allows to define the right Cauchy–Green tensor $\mathbf{C} = \mathbf{F}^{\mathrm{T}}\mathbf{F}$.

Let the free energy Ψ per unit reference volume be given by the function $\Psi = \hat{\Psi}(\mathbf{C})$. For a hyperelastic unconstrained material the second Piola–Kirchhoff stress $\mathbf{S}$ and the related Cauchy stress $\boldsymbol{\sigma}$ as well as fourth-order tangent tensor $\mathbb{C}$ are

$$\mathbf{S} = 2\frac{\partial\,\hat{\Psi}}{\partial\mathbf{C}}\,, \quad \boldsymbol{\sigma} = J^{-1}\mathbf{F}\mathbf{S}\mathbf{F}^{\mathrm{T}}, \quad \mathbb{C} = 2\frac{\partial\mathbf{S}}{\partial\mathbf{C}} = 4\frac{\partial^2\,\hat{\Psi}}{\partial\mathbf{C}\partial\mathbf{C}}\,. \tag{1}$$

We assume that the reference configuration $\mathcal{B}_0$ is associated with an energy- and stress-free state of the material, i.e. $\hat{\Psi}(\mathbf{I}) = 0$ and $\mathbf{S}(\mathbf{I}) = \mathbf{0}$.

2.2. Averaging of the fibre energy

We propose a new method to approximate the free energy density Ψ_{f} of a network or ensemble of statistically distributed fibres characterised by the fibre strain–energy density function[1] ψ. We assume that ψ is expressed in terms of the fibre square stretch $\Lambda = \lambda^2$. To this end, we introduce the expectation operator $\mathrm{E}[\,\cdot\,]$ to express the macroscopic energy Ψ_{f} as an integral of the microscopic energy ψ, i.e.

$$\Psi_{\mathrm{f}} = \nu_{\mathrm{f}}\mathrm{E}[\psi]\,, \tag{2}$$

where ν_{f} is a constant used for the energetic scale equivalence, essentially akin to a 'fibre density'. If it exists a function $\Lambda_{\boldsymbol{N}} : \mathbb{E} \to \mathbb{R}$, $\boldsymbol{N} \mapsto \Lambda$ that for each macroscopic deformation $\mathbf{C}$ returns the real scalar square stretch Λ of a fibre that is initially oriented along the unit vector $\boldsymbol{N}$ within the Euclidean vector space $\mathbb{E}$, the expectation $\mathrm{E}[\psi]$ can be evaluated as

$$\mathrm{E}[\psi] = \int_{\mathcal{S}} \psi(\Lambda_{\boldsymbol{N}}(\boldsymbol{z}))\,\mathrm{d}P_{\boldsymbol{N}}(\boldsymbol{z})\,, \tag{3}$$

where $P_{\boldsymbol{N}}$ models the initial fibre orientation distribution in the reference state. Although (3) has become the standard approach for averaging fibre energies, the intermediate change of variables to express the stretch dependent energy ψ as a function of orientation $\boldsymbol{N}$, is in general not required. More generally, and particularly not requiring the existence of $\Lambda_{\boldsymbol{N}}$, the expectation can be expressed as [18]

$$\mathrm{E}[\psi] = \int_{\mathbb{R}_{>0}} \psi(x)\,\mathrm{d}P_{\Lambda}(x)\,, \tag{4}$$

where P_{Λ} is the stretch distribution. In almost all cases relevant for the mechanics of tissues and materials with continuously distributed fibres, the latter can be expressed in terms of a corresponding density function p_{Λ}, so that Eq. (4) can be written as

$$\mathrm{E}[\psi] = \int_{\Lambda_{\min}}^{\Lambda_{\max}} \psi(x)\,p_{\Lambda}(x)\,\mathrm{d}x\,, \tag{5}$$

with limits $0 < \Lambda_{\min} < \Lambda_{\max} < \infty$ that reflect the extremal values of the square stretch appearing within the network. In fact, p_{Λ} may degenerate or be non-existent in special cases, e.g. in the case of discrete single fibre directions or if all stretches concentrate at a single value implying $\Lambda_{\min} = \Lambda_{\max}$. For the realm of this paper, and in particular for the formulation of the Gauss quadrature proposed in Section 3 we will assume validity of the representation (5) and deal with exceptions separately (cf. Remark 1).

[1] For fibres the 'density' ψ may represent the energy per unit volume or per unit length, depending on whether fibres are modelled as three or one-dimensional structures. The factor ν_{f} in Eq. (2) is accordingly dimensionless or has units of $(\text{area})^{-1}$, respectively.

If the function Λ_N exists, the two Eqs. (3) and (5) both evaluate the integral $\mathrm{E}[\cdot]$. An important example concerns the affine case dealt with in Section 4, for which $\Lambda_N = \boldsymbol{N}\cdot\mathbf{C}\boldsymbol{N}$. In view of the unit sphere $\mathcal{S}$ representing the integration domain of Eq. (3), one might want to parametrise $\boldsymbol{N}$ in terms of spherical angles ϕ and θ. Accordingly, one finds the equality

$$\mathrm{E}[\cdot] = \int_{\mathbb{R}_{>0}} \cdot \,\mathrm{d}P_\Lambda(x) = \int_{\mathcal{S}} \cdot \,\mathrm{d}P_N(\boldsymbol{z}) = \frac{1}{4\pi}\int_0^{2\pi}\int_0^{\pi} \cdot\ \rho(\phi,\theta)\,\sin(\theta)\mathrm{d}\theta\,\mathrm{d}\phi\,, \tag{6}$$

where "$\cdot$" is the placeholder for the integrand, that naturally needs to be expressed in terms of the integration variables. For completeness $\rho(\phi,\theta)$ is a common orientation density that quantifies the weight of fibre material aligned along $\boldsymbol{N}$, and that is normalised such that $\mathrm{E}[1] = 1$.

In practise, if the transformation (6) is admissible, i.e. given an integrand that can be expressed as a function $f(\boldsymbol{N}(\phi,\theta))$ and provided a continuous fibre distribution $\rho(\phi,\theta)$, this integral is typically approximated using a spherical cubature rule, i.e. [see e.g. 3]

$$\mathrm{E}[f(\boldsymbol{N})] \approx \mathrm{SC}[f(\boldsymbol{N})] = \sum_{k=1}^{n} f(\boldsymbol{N}_k)\,\rho(\phi_k,\theta_k)\,W_k \tag{7}$$

with integration points $\{\boldsymbol{N}_k\}$ on the unit sphere, corresponding to the pairs $\{(\phi_k,\theta_k)\}$, and weights $\{W_k\}$. Indeed the weights $\{W_k\}$ are typically not accounting for the fibre distribution $\rho(\phi,\theta)$ that therefore practically becomes part of the integrand. Formally one may of course consider $\tilde{W}_k = \rho(\phi_k,\theta_k)W_k$ as new weights, but we emphasise that as a consequence of the approximative character of (7) they usually violate the condition $\mathrm{E}[1] = \sum_k \tilde{W}_k$, and need to be re-normalised (cf. Remark 3).

Among a generally wide choice of spherical cubature rules of the type (7), applications in mechanics have favoured integration schemes that satisfy additional criteria, e.g. on symmetry or sign of the weights [11,17,23,24]. Among those schemes, a spherical t-design [25,26] will be considered in Section 5.1. Moreover, in order to achieve a costly but highly accurate approximation of Eq. (6) that will serve as ground truth for our further developments and benchmarks, a high-order Lebedev quadrature [27,28] was used. Both selected methods integrate polynomials up to a certain degree t exactly.

3. Gauss quadrature of stretch dependent constitutive laws

The alternative form of the free energy representation (5) suggests that if the stretch distribution is known, the expectation can be approximated by one of the well-established quadrature rules that exist for univariate integrals. Quadrature rules of the Gaussian type are commonly applied for a wide range of problems and in this section we will show that classical Gauss quadrature is particularly suitable to evaluate the expectation of the free energy (5) since the integration points and weights can be associated with the stretch distribution P_Λ.

3.1. n-Point Gauss quadrature

Applying Gauss-type quadrature to evaluate the integral[2] (5), the n-point approximate reads [19,29,30]

$$\boxed{\mathrm{E}[\psi] = \int_{\Lambda_{\min}}^{\Lambda_{\max}} \psi(x)\,p_\Lambda(x)\,\mathrm{d}x \;\approx\; \mathrm{GI}[\psi] = \sum_{k=1}^{n}\psi(x_k)w_k\,,} \tag{8}$$

where $\{x_k\}$ and $\{w_k\}$ are the integration points and corresponding weights, respectively. It can be shown Appendix A that (i) the Gauss integration is exact for polynomials of degree $m \le 2n-1$, (ii) that the integration points $\{x_k\}$ lie in the range $[\Lambda_{\min}, \Lambda_{\max}]$ and (iii) the weights $\{w_k\}$ are positive [29]. Importantly, in this type of quadrature only the function $\psi(x)$ is evaluated at $\{x_k\}$, while the 'weight function' $p_\Lambda(x)$ affects their positions and the weights w_k.

The integration points $\{x_k\}$ are the roots of the nth orthogonal polynomial P_n (Section 3.2) corresponding to p_Λ and the weights $\{w_k\}$ calculate as Appendix A

$$w_i = \mathrm{E}\left[\prod_{j\neq i}\frac{x-x_j}{x_i-x_j}\right], \quad i = 1,2,\ldots,n. \tag{9}$$

[2] Gaussian quadrature may be directly applied to the more general integral (4) [19].

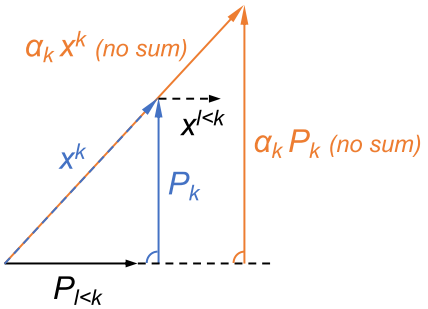

Fig. 1. Illustration of the Gram–Schmidt orthogonalisation process (12) and relationship (13).

Notably, in the common but here irrelevant case, where the weight function is constant P_n are the Legendre polynomials.

3.2. Orthogonal polynomials corresponding to p_Λ

The orthogonal polynomials $\{P_k\}$ are defined with respect to the inner product (in an infinite vector space) [cp. 31], which in the specific problem is given by the expectation (5),

$$\langle f, g\rangle = \int_{\Lambda_{\min}}^{\Lambda_{\max}} f(x)\, g(x)\, p_\Lambda(x)\, \mathrm{d}x = \mathrm{E}[f\, g]\ , \tag{10}$$

such that

$$\langle P_n, x^k\rangle = \mathrm{E}\left[P_n\, x^k\right] = 0, \ \text{ for all } k < n. \tag{11}$$

Following the idea of the Gram–Schmidt (orthogonalisation) process, starting from the standard basis for polynomials $\{x^k\}$ and definition of $P_0 = 1$, one can compute [see e.g. 31]

$$\begin{aligned}
P_0 &= 1,\\
P_1 &= x - \frac{\langle x,\, P_0\rangle}{\langle P_0,\, P_0\rangle} P_0,\\
P_2 &= x^2 - \frac{\langle x^2,\, P_0\rangle}{\langle P_0,\, P_0\rangle} P_0 - \frac{\langle x^2,\, P_1\rangle}{\langle P_1,\, P_1\rangle} P_1,\\
&\ \ \vdots\\
P_n &= x^n - \sum_{k=0}^{n-1} \frac{\langle x^n,\, P_k\rangle}{\langle P_k,\, P_k\rangle} P_k\\
&= x^n - (\text{projections of } x^n \text{ onto } P_k \text{ for } k < n)
\end{aligned} \tag{12}$$

to obtain in the kth step P_k as that part of x^k that is perpendicular to all P_l for $l < k$. Hence, using in the kth step instead of x^k an arbitrary kth order polynomial $\sum_{l=0}^{k} \alpha_l x^l$ with leading coefficient $\alpha_k = 1$ yields the same orthogonal polynomial P_k because all $\{\alpha_l x^l\}_{l<k}$ are linear combinations of $\{P_l\}_{l<k}$ and therefore naturally perpendicular to P_k. In case of an arbitrary leading coefficient α_k one has the relationship (cp. Fig. 1)

$$\tilde{P}_k = \sum_{l=0}^{k} \alpha_l x^l - (\text{projections of } \sum_{l=0}^{k} \alpha_l x^l \text{ onto } P_l \text{ for } l < k) = \alpha_k P_k. \tag{13}$$

3.3. $\{P_k\}$ As functions of the moments of p_Λ

According to (10) and (12), calculation of the orthogonal polynomials (12) requires computing the inner products

$$\langle x^k, P_l\rangle = \mathrm{E}\left[x^k\, P_l\right], \quad l < k. \tag{14}$$

The latter are integrals of polynomials in x because P_l are polynomials in x, and can accordingly be expressed as a finite weighted sum of $\{\mathrm{E}\left[x^k\right]\}$, i.e. integrals of integer powers x^k. As a consequence, knowledge of the integrals $\{\mathrm{E}\left[x^k\right]\}$ implies a closed-form solution for $\{P_k\}$. In fact, given the definition (6), $\mathrm{E}\left[x^k\right]$ can be identified as the kth *raw moment* of the square stretch distribution, which we will denote as

$$\mu_k = \mathrm{E}\left[x^k\right]. \tag{15}$$

Expressing orthogonal polynomials in terms of raw moments is an established process, and one can derive the following determinant formula to determine the set $\{Q_k\}$ of orthogonal polynomials [31, Eq. 2.2.6]

$$Q_n = \begin{vmatrix} 1 & \mu_1 & \mu_2 & \mu_3 & \dots & \mu_n \\ \mu_1 & \mu_2 & \mu_3 & \mu_4 & \dots & \mu_{n+1} \\ \mu_2 & \mu_3 & \mu_4 & \mu_5 & \dots & \mu_{n+2} \\ \vdots & & & & & \vdots \\ \mu_{n-1} & \mu_n & \mu_{n+1} & \mu_{n+2} & \dots & \mu_{2n-1} \\ 1 & x & x^2 & x^3 & \dots & x^n \end{vmatrix}, \tag{16}$$

to be understood as a cofactor expansion along the last row. One can easily verify that Q_n is indeed orthogonal to all $\{Q_k\}_{k<n}$: Since each $\{Q_k\}_{k<n}$ is a linear combination of $\{x^k\}_{k<n}$, it suffices to confirm that Q_n is orthogonal to all $\{x^k\}_{k<n}$, i.e. that

$$\langle Q_n, x^k \rangle = \mathrm{E}\left[\begin{vmatrix} 1 & \dots & \mu_n \\ \vdots & & \vdots \\ \mu_{n-1} & \dots & \mu_{2n-1} \\ 1 & \dots & x^n \end{vmatrix} x^k \right] = \mathrm{E}\left[\begin{vmatrix} 1 & \dots & \mu_n \\ \vdots & & \vdots \\ \mu_{n-1} & \dots & \mu_{2n-1} \\ x^k & \dots & x^{k+n} \end{vmatrix} \right] = 0, \quad k < n, \tag{17}$$

which is satisfied, because after integration the last and $(k+1)$th row in the determinant are identical, so that the determinant evaluates to 0.

The polynomials Q_n are scalar multiples of the orthogonals P_n, and in view of Eq. (13) we set $\tilde{P}_n = Q_n$, so that

$$Q_n = G_{2n-2,\mu} P_n, \quad G_{2n-2,\mu} = \begin{vmatrix} 1 & \mu_1 & \mu_2 & \mu_3 & \dots & \mu_{n-1} \\ \mu_1 & \mu_2 & \mu_3 & \mu_4 & \dots & \mu_n \\ \mu_2 & \mu_3 & \mu_4 & \mu_5 & \dots & \mu_{n+1} \\ \vdots & & & & & \vdots \\ \mu_{n-1} & \mu_n & \mu_{n+1} & \mu_{n+2} & \dots & \mu_{2n-2} \end{vmatrix}, \tag{18}$$

where $G_{2n-2,\mu}$ plays the role of α_n as the leading coefficient arising from a cofactor expansion of the determinant formula for Q_n.

Alternatively introducing the signed distance of x from the mean μ_1 as

$$\bar{x} = x - \mu_1, \tag{19}$$

one can express the orthogonal polynomial P_k in terms of the *central moments*

$$\bar{\mu}_k = \mathrm{E}\left[\bar{x}^k\right], \tag{20}$$

because $(x-\mu_1)^k$ has the same leading coefficient as x^k and using the arguments that led to Eq. (13). In analogy to Eq. (16) one finds Q_n as

$$Q_n = \begin{vmatrix} 1 & 0 & \bar{\mu}_2 & \bar{\mu}_3 & \dots & \bar{\mu}_n \\ 0 & \bar{\mu}_2 & \bar{\mu}_3 & \bar{\mu}_4 & \dots & \bar{\mu}_{n+1} \\ \bar{\mu}_2 & \bar{\mu}_3 & \bar{\mu}_4 & \bar{\mu}_5 & \dots & \bar{\mu}_{n+2} \\ \vdots & & & & & \vdots \\ \bar{\mu}_{n-1} & \bar{\mu}_n & \bar{\mu}_{n+1} & \bar{\mu}_{n+2} & \dots & \bar{\mu}_{2n-1} \\ 1 & \bar{x} & \bar{x}^2 & \bar{x}^3 & \dots & \bar{x}^n \end{vmatrix}, \tag{21}$$

where in analogy to Eq. (18) $Q_n = G_{2n-2,\bar{\mu}} P_n$ and we note that indeed $G_{2n-2,\bar{\mu}} = G_{2n-2,\mu}$. Since for determining the roots of the orthogonal polynomials their normalisation and scaling is irrelevant, we will henceforth focus on their form Q_n (21).

Explicitly for the first four orthogonal polynomials $\{Q_k\}$ one finds

$$\begin{aligned} Q_0 &= 1, \\ Q_1 &= \bar{x}, \\ Q_2 &= \bar{\mu}_2 \bar{x}^2 - \bar{\mu}_3 \bar{x} - \bar{\mu}_2^2, \\ Q_3 &= a \bar{x}^3 + b \bar{x}^2 + c \bar{x} + d, \end{aligned} \tag{22}$$

where the coefficients $\{a, b, c, d\}$ are given by

$$\begin{aligned} a &= \bar{\mu}_2\bar{\mu}_4 - \bar{\mu}_2^3 - \bar{\mu}_3^2, \\ b &= \bar{\mu}_2^2\bar{\mu}_3 - \bar{\mu}_2\bar{\mu}_5 + \bar{\mu}_3\bar{\mu}_4, \\ c &= \bar{\mu}_2^2\bar{\mu}_4 - \bar{\mu}_2\bar{\mu}_3^2 + \bar{\mu}_3\bar{\mu}_5 - \bar{\mu}_4^2, \\ d &= \bar{\mu}_2^2\bar{\mu}_5 - 2\bar{\mu}_2\bar{\mu}_3\bar{\mu}_4 + \bar{\mu}_3^3. \end{aligned} \tag{23}$$

3.4. Integration points $\{x_k\}$ as functions of the moments of p_Λ

In view of the fact that there exists no general closed-form solution for the quintic (and thus any higher order) equation, the roots of Q_n and therefore the integration points $\{x_k\}$ may generally have to be computed numerically. In the following we will therefore focus on the well known closed-form solutions for the roots of polynomials of degree $n \leq 3$.

Since the expression for the orthogonal polynomials $\{Q_k\}$ (22) depends on $\bar{x}$, i.e. the position of x relative to μ_1, it is useful to likewise determine the location of the roots $\{x_k\}$ relative to μ_1. Therefore analogous to Eq. (19) we define $\{\bar{x}_k\}$ such that

$$\boxed{x_k = \bar{x}_k + \mu_1\,.} \tag{24}$$

Obviously for $n = 1$, the single root of P_1 or equivalently Q_1 (22) is $\bar{x}_1 = 0$, i.e. $x_1 = \mu_1$. In case $n = 2$ the quadratic formula helps determine $x_{1,2} = \mu_1 + \bar{x}_{1,2}$ with

$$\boxed{\bar{x}_{1,2} = \frac{\bar{\mu}_3 \mp \sqrt{4\bar{\mu}_2^3 + \bar{\mu}_3^2}}{2\bar{\mu}_2}} \tag{25}$$

as the two roots of P_2 and Q_2 (22). For the $n = 3$ closed-form solution, the roots $x_k = \mu_1 + \bar{x}_k$ of P_3 and Q_3 (22) can be expressed by means of Cardano's formula, so that

$$\boxed{\bar{x}_k = \frac{\mathcal{I}_1 + 2\sqrt{\mathcal{A}}C_k}{3}\,, \quad C_k = \cos\left(\frac{\vartheta + 2\pi k}{3}\right), \quad k = 1, 2, 3,} \tag{26}$$

where

$$\mathcal{A} = \mathcal{I}_1^2 - 3\mathcal{I}_2\,, \quad \mathcal{B} = \mathcal{I}_1^3 - \frac{9}{2}\mathcal{I}_1\mathcal{I}_2 + \frac{27}{2}\mathcal{I}_3\,, \quad \vartheta = \arccos\left(\frac{\mathcal{B}}{\mathcal{A}^{3/2}}\right) \tag{27}$$

are defined in terms of the dedicated invariant expressions

$$\mathcal{I}_1 = -\frac{b}{a}\,, \quad \mathcal{I}_2 = \frac{c}{a}\,, \quad \mathcal{I}_3 = -\frac{d}{a}\,, \tag{28}$$

which in turn can be written in terms of the central moments $\bar{\mu}_k$, $k = 1, 2, \ldots, 5$, by use of the auxiliary variables (23). We note that because the roots are real, it can be shown that $\mathcal{A} \geq 0$ and $\mathcal{B}/\mathcal{A}^{3/2} \in (-1, 1)$. Finally, we emphasise that the expressions (28) must not be confused with the principal strain invariants.

Remark 1 (*Single Stretch Value*)**.** The determination of the roots for the $n > 1$ cases, requires a variance $\bar{\mu}_2 > 0$, i.e. a stretch distribution that does not concentrate all stretches at a single value Λ_{single}. This technical detail may

be simply circumvented by a case distinction in Eq. (5) and appreciation of the associated trivial solution, i.e. in this case $\mathrm{E}[\psi] = \psi(\Lambda_{\text{single}})$. Alternatively, one may add small perturbations to the stretch Λ_{single} in the numerical solution, which in view of a stable problem can be considered reasonable as this only leads to small variations in the result.

3.5. Weights $\{w_k\}$ as functions of the moments of p_Λ

Given the integration points $\{x_k\}$ the computation of the weights (9) again requires to determine integrals of polynomials in x, which in turn we have identified in terms of moments of the stretch distribution. Therefore the weights (9) can generally be expressed as functions of the moments as well. For the n-point quadratures with $n \leq 3$ for which closed-form solutions for the integration points have been derived in the previous section (24)–(26) we will now explicitly state the corresponding weights.

In case $n = 1$ the single weight is 1. In case $n = 2$ insertion of the integration points $\{x_1, x_2\}$ given by Eq. (24), (25) into the formula for the weights (9) yields

$$\boxed{w_{1,2} = \frac{1}{2} \pm \frac{\bar{\mu}_3}{2\sqrt{4\bar{\mu}_2^3 + \bar{\mu}_3^2}}}, \tag{29}$$

which matches with the intuition that for a positive skewness $\bar{\mu}_3 > 0$, i.e. a stretch distribution with a tail to the right, more weight should be put to the left integration point x_1 that is then closer to the mean μ_1 (see Eq. (25)) and vice versa. If the skewness is zero, the distribution is symmetric, the integration points have equal distance from the mean and the weights are equal. For $n = 3$, using the transformations (19) and (24), the weights (9) can be written as

$$w_k = \mathrm{E}\left[\frac{(\bar{x} - \bar{x}_j)(\bar{x} - \bar{x}_l)}{(\bar{x}_k - \bar{x}_j)(\bar{x}_k - \bar{x}_l)}\right], \quad k \neq j \neq l \neq k, \tag{30}$$

where we used again the notation $\bar{x} = x - \mu_1$ and $\bar{x}_k = x_k - \mu_1$. Taking into account that $\mathrm{E}[\bar{x}] = 0$ this simplifies as

$$\boxed{w_k = \frac{\bar{\mu}_2 + \bar{x}_j \bar{x}_l}{v_k}, \quad v_k = (\bar{x}_k - \bar{x}_j)(\bar{x}_k - \bar{x}_l), \quad k \neq j \neq l \neq k}, \tag{31}$$

where $\{\bar{x}_k\}$ is given in Eq. (26), and k runs from 1 to 3.

3.6. Derivatives of the approximated expectation

The stretch distribution generally depends on the macroscopic deformation expressed through $\mathbf{C}$. The same holds for its moments and correspondingly for the integration points and weights, which define the Gauss quadrature of the averaged free energy $\mathrm{E}[\psi] \approx \mathrm{GI}[\psi]$ (8). Since the latter defines the free energy density of the material Ψ, e.g. through Eq. (2) or, as exemplified later in Sections 5.2.2 and 5.2.3, the calculation of stress and stiffness according to Eq. (1) requires the computation of first and second derivatives of $\mathrm{GI}[\psi]$ with respect to $\mathbf{C}$. Assuming that the integration points $\{x_k\}$ and corresponding weights $\{w_k\}$ can be expressed as functions of $\mathbf{C}$, these derivatives of the quadrature rule (8) are

$$\frac{\partial \mathrm{GI}[\psi]}{\partial \mathbf{C}} = \sum_{k=1}^{n} \psi'(x_k) w_k \frac{\partial x_k}{\partial \mathbf{C}} + \psi(x_k) \frac{\partial w_k}{\partial \mathbf{C}} \tag{32}$$

and

$$\begin{aligned} \frac{\partial \mathrm{GI}[\psi]}{\partial \mathbf{C}} = \sum_{k=1}^{n} & \psi''(x_k) w_k \frac{\partial x_k}{\partial \mathbf{C}} \otimes \frac{\partial x_k}{\partial \mathbf{C}} \\ & + \psi'(x_k) \left(\frac{\partial x_k}{\partial \mathbf{C}} \otimes \frac{\partial w_k}{\partial \mathbf{C}} + \frac{\partial w_k}{\partial \mathbf{C}} \otimes \frac{\partial x_k}{\partial \mathbf{C}} + w_k \frac{\partial^2 x_k}{\partial \mathbf{C} \partial \mathbf{C}} \right) \\ & + \psi(x_k) \frac{\partial^2 w_k}{\partial \mathbf{C} \partial \mathbf{C}}, \end{aligned} \tag{33}$$

where $x_k = \mu_1 + \bar{x}_k$. Since the integration points $\{x_k\}$ and weights $\{w_k\}$ have already been derived as functions of the moments $\{\mu_1, \bar{\mu}_2, \bar{\mu}_3, \ldots\}$, use of the first and second derivatives of these moments (Sections 4.3 and 4.4) along with the chain rule of differentiation

$$y_{,\mathbf{C}} = \sum_{M \in \{\mu_1, \bar{\mu}_2, \bar{\mu}_3\}} y_{,M} M_{,\mathbf{C}} \quad \text{for } y \in \{x_k, w_k\}, \tag{34}$$

provides the expressions $\{x_{k,\mathbf{C}}\}$ and $\{w_{k,\mathbf{C}}\}$ as well as $\{x_{k,\mathbf{CC}}\}$ and $\{w_{k,\mathbf{CC}}\}$. While for $n = 1$ ($x_1 = \mu_1$) and $n = 2$ (Eq. (24), (25)) these expressions are straightforward, they are provided in Appendix B for $n = 3$.

Remark 2 (*Numeric Computation of Stress and Tangent Tensors*)**.** Alternative to the analytic approach presented in Section 3.6 numeric differentiation schemes [see e.g. 32,33] applied to the free energy Ψ may be used to compute the stress and tangent tensor components, in particular for the cases, where the integration points (i.e. the roots of P_n) are determined numerically, i.e. most likely for any case $n > 3$.

4. Application to anisotropic affine networks

The Gauss quadrature averaging is next specified for the special case of affine fibre kinematics. The assumption of affinity establishes for any fixed state of deformation expressed through $\mathbf{C} = \mathbf{F}^{\mathrm{T}}\mathbf{F}$ a deterministic relation between fibre stretch and initial orientation, and thus allows defining the function $\Lambda_{\boldsymbol{N}} : \mathbb{E} \to \mathbb{R}$, $\boldsymbol{N} \mapsto \Lambda$. Consequently, the square stretch distribution P_Λ and its density p_Λ can be exclusively expressed in terms of $\mathbf{C}$ and the orientation distribution $\rho(\phi, \theta)$ by use of suitable variable transformations [4,34,35]. Moreover, as resumed in Section 2.2 the expectation $\mathrm{E}[\cdot]$ can be equivalently evaluated as either an integral over the stretch distribution or over the unit sphere (6). This equivalence allows exactly determining the moments (20) by means of well established methods, in terms of either strain invariants in the isotropic case [4,36] or in terms of generalised structural tensors in the general, anisotropic case of non-uniform fibre orientation distributions [4,37]. Here, we focus on the second of these cases, which has gained particular importance for formulating constitutive models of soft collagenous biological tissues.

4.1. Preliminaries

4.1.1. Affine kinematics

If the fibres are assumed to transform like infinitesimal vectorial line elements of the macroscopic material considered as a continuous body, their change in squared end-to-end length is defined by the macroscopic deformation gradient $\mathbf{F}$ through the affine mapping, so that

$$\Lambda := \Lambda_{\boldsymbol{N}} = \|\mathbf{F}\boldsymbol{N}\|^2 = \boldsymbol{N} \cdot \mathbf{C}\boldsymbol{N}. \tag{35}$$

This deterministic relation between initial orientation, macroscopic deformation and the microscopic fibre stretch also sets the limits $\Lambda_{\min}$ and $\Lambda_{\max}$ of the (square) stretch distribution (5), which result as the minimum and maximum eigenvalue of $\mathbf{C}$ in this case.

4.1.2. Cartesian components

For the sake of simplicity and in view of the implementation into computer codes, we use index-notation in this section, together with the Einstein summation-convention to express vectors, second and higher order tensors through their Cartesian components referring to a basis formed by a fixed orthonormal set of vectors $\{\boldsymbol{e}_1, \boldsymbol{e}_2, \boldsymbol{e}_3\}$. Consequently we will address vectors $\boldsymbol{v} = v_i \boldsymbol{e}_i$, second order tensors $\boldsymbol{T} = T_{ij} \boldsymbol{e}_i \otimes \boldsymbol{e}_i$ and in general nth order tensors

$$\mathbb{A} = A_{i\ldots t} \boldsymbol{e}_i \otimes \ldots \otimes \boldsymbol{e}_t \tag{36}$$

by just their components, i.e. v_i, T_{ij} and in general $A_{i\ldots t}$.

4.1.3. Generalised structural tensors

The nth even order generalised structural tensor is defined as [38]

$$\mathbb{H}_n = \mathrm{E}\left[\underbrace{\boldsymbol{N}\otimes\ldots\otimes\boldsymbol{N}}_{n\ \text{copies}}\right]. \tag{37}$$

The Cartesian components of $\mathbb{H}_n$ with respect to the orthonormal basis $\{\boldsymbol{e}_i\}$ thus read

$$\underbrace{H_{ij\ldots st}}_{2n} = \mathrm{E}\left[\underbrace{N_i N_j \ldots N_s N_t}_{2n}\right], \tag{38}$$

where $N_i = \boldsymbol{N}\cdot\boldsymbol{e}_i$. It is observed that the value of the component $H_{ij\ldots st}$ depends only on the number of occurrences p, q, r of the indices 1, 2, 3, respectively. Hence for computation and storage it is reasonable to introduce [39]

$$H_{p,q,r} = \mathrm{E}\left[N_1^p N_2^q N_3^r\right], \tag{39}$$

where the sum of p, q, r is equal to the number of indices in the representation (38) and therefore the (even) order $2n$ of the structural tensor. In view of Eq. (6), it can be concluded that given a fibre orientation distribution $\rho(\phi,\theta)$ these components calculate as

$$H_{p,q,r} = \frac{1}{4}\int_0^{2\pi}\int_0^{\pi} \cos^p(\phi)\sin^q(\phi)\sin^{p+q+1}(\theta)\cos^r(\theta)\,\rho(\phi,\theta)\,\mathrm{d}\theta\,\mathrm{d}\phi\,, \tag{40}$$

where we used the definition of the spherical angles according to which

$$\boldsymbol{N} = N_i\boldsymbol{e}_i = \cos(\phi)\sin(\theta)\boldsymbol{e}_1 + \sin(\phi)\sin(\theta)\boldsymbol{e}_2 + \cos(\theta)\boldsymbol{e}_3\,. \tag{41}$$

While for special cases of $\rho(\phi,\theta)$ the components (40) can be calculated analytically [cf. e.g. 39], the general case requires numerical integration, which typically uses the cubature rule (7), i.e.

$$H_{p,q,r} = \mathrm{E}\left[N_1^p N_2^q N_3^r\right] \approx \mathrm{SC}\left[N_1^p N_2^q N_3^r\right] = \sum_{k=1}^{n} (\boldsymbol{N}_k)_1^p (\boldsymbol{N}_k)_2^q (\boldsymbol{N}_k)_3^r \underbrace{\rho(\phi_k,\theta_k)\,W_k}_{=\tilde{W}_k} \tag{42}$$

for integration points $\{\boldsymbol{N}_k\}$, equivalently expressed through pairs of spherical angles $\{(\phi_k,\theta_k)\}$, on the unit sphere and weights $\{W_k\}$.

Another important property of generalised structural tensors is that higher order tensors contain all information about lower order tensors, and in particular that the tensors of order $2n$ result from those of $2(n+1)$ by simple contraction with the second order identity tensor. For the components (38) this leads to [cf. 38]

$$\underbrace{H_{ij\ldots st}}_{\text{order } 2n} = \mathrm{E}\left[N_i N_j \ldots N_s N_t \underbrace{N_u N_v \delta_{uv}}_{=1}\right] = \underbrace{H_{ij\ldots stuv}}_{\text{order } 2(n+1)}\ \delta_{uv}\,, \tag{43}$$

which we understand to include $H_{st}\delta_{st} = 1$ and $H_{stuv}\delta_{uv} = H_{st}$ for $n = 0$ and $n = 1$, respectively.

Remark 3 (*Consistency of $H_{ij\ldots st}$*)**.** As already mentioned, due to the numerical error of spherical cubature, the new weights $\{\tilde{W}_k\}$ in Eq. (42) obtained in this way usually do not satisfy the normalisation condition $\mathrm{E}[1] = 1$, i.e. $\sum_k \tilde{W}_k = 1$. Consequently, determining $H_{ij\ldots st}$ through Eq. (42) usually violates the important properties (43), i.e. in particular $H_{st}\delta_{st} = 1$, making the structural tensors inconsistent. A simple solution to overcome this issue is to renormalise the new weights $\{\tilde{W}_k\}$ as

$$\tilde{W}_k^* = \frac{\tilde{W}_k}{\sum_{k=1}^{n}\tilde{W}_k}, \quad k = 1, 2, \ldots, n, \tag{44}$$

and to use $\tilde{W}_k^*$ instead of $\tilde{W}_k$ in Eq. (42). Such a procedure is reasonable as it just shifts the numerical error.

For the proposed GI method, this consistency is very important as otherwise the formulae for the moments (48) may yield unreasonable results leading to nonsensical Gauss integration points (Section 3.4), e.g., situated outside of the interval $[\Lambda_{\min}, \Lambda_{\max}]$ in which they must fall.

4.2. Moments of the affine stretch distribution

In terms of the components of $\mathbf{C}$ and $\boldsymbol{N}$, the affine square stretch (35) reads

$$\Lambda = \boldsymbol{N} \cdot \mathbf{C}\boldsymbol{N} = C_{ij} N_i N_j \,. \tag{45}$$

According to the definition of the first raw moment (15) one finds

$$\mu_1 = \mathrm{E}\left[\Lambda\right] = \mathrm{E}\left[C_{ij} N_i N_j\right] = C_{ij} H_{ij}. \tag{46}$$

The definition of the central moments (20) further yields [4]

$$\begin{aligned} \bar{\mu}_k &= \mathrm{E}\left[(C_{ij} N_i N_j - \mu_1)^k\right] = \mathrm{E}\left[((C_{ij} - \mu_1 \delta_{ij}) N_i N_j)^k\right] \\ &= \underbrace{(C_{ij} - \mu_1 \delta_{ij}) \ldots (C_{mn} - \mu_1 \delta_{mn})}_{k \text{ copies}} H_{ij\ldots mn} \,, \end{aligned} \tag{47}$$

where δ_{ij} is the Kronecker symbol so that for the second equality in Eq. (47) we could use that $\|\boldsymbol{N}\|^2 = \delta_{ij} N_i N_j = 1$. Explicitly the first five relevant moments read

$$\boxed{\begin{aligned} \mu_1 &= C_{ij} H_{ij}, \\ \bar{\mu}_2 &= \tilde{C}_{ij} \tilde{C}_{kl} H_{ijkl} \,, \\ \bar{\mu}_3 &= \tilde{C}_{ij} \tilde{C}_{kl} \tilde{C}_{mn} H_{ijklmn} \,, \\ \bar{\mu}_4 &= \tilde{C}_{ij} \tilde{C}_{kl} \tilde{C}_{mn} \tilde{C}_{st} H_{ijklmnst} \,, \\ \bar{\mu}_5 &= \tilde{C}_{ij} \tilde{C}_{kl} \tilde{C}_{mn} \tilde{C}_{st} \tilde{C}_{uv} H_{ijklmnstuv} \,, \end{aligned}} \tag{48}$$

where

$$\tilde{C}_{ij} = C_{ij} - \mu_1 \delta_{ij} \,. \tag{49}$$

Remark 4 (*Isotropic Materials*)**.** We note that for uniform fibre distributions, all moments can be expressed in terms of polynomials of invariants of $\mathbf{C}$, as outlined in [4]. Terms up to the 10th moment have been provided before [see 36].

4.3. Derivatives of the moments with respect to $\mathbf{C}$

As $\mu_1 = C_{kl} H_{kl}$ it follows that

$$\frac{\partial \mu_1}{\partial C_{ij}} = \delta_{ki} \delta_{lj} H_{kl} = H_{ij} \,, \tag{50}$$

and consequently $\partial^2 \mu_1 / (\partial C_{st} \partial C_{ij}) = 0$. Considering definition (49), for $\bar{\mu}_2 = \tilde{C}_{mn} \tilde{C}_{op} H_{mnop}$ one can derive

$$\begin{aligned} \frac{\partial \bar{\mu}_2}{\partial C_{ij}} &= \left(\frac{\partial \tilde{C}_{mn}}{\partial C_{ij}} \tilde{C}_{op} + \tilde{C}_{mn} \frac{\partial \tilde{C}_{op}}{\partial C_{ij}} \right) H_{mnop} \\ &= 2(\delta_{mi} \delta_{nj} + H_{ij} \delta_{mn}) \tilde{C}_{op} H_{mnop} \\ &= 2 \tilde{C}_{op} (H_{ijop} + H_{ij} H_{op}) = 2 \tilde{C}_{op} H_{ijop} \,. \end{aligned} \tag{51}$$

Here, to obtain the second equality, the symmetry of H_{mnop} was exploited, and that its value is independent of the ordering of its indices (cf. Eq. (39)). The third and final equality holds due to the property (43) and because $\tilde{C}_{op} H_{op} = \bar{\mu}_1 = 0$, respectively. From Eq. (51) one can further derive

$$\begin{aligned} \frac{\partial^2 \bar{\mu}_2}{\partial C_{st} \partial C_{ij}} &= 2(\delta_{os} \delta_{pt} + H_{st} \delta_{op}) H_{ijop} \\ &= 2(H_{ijst} + H_{st} H_{ij}) \,. \end{aligned} \tag{52}$$

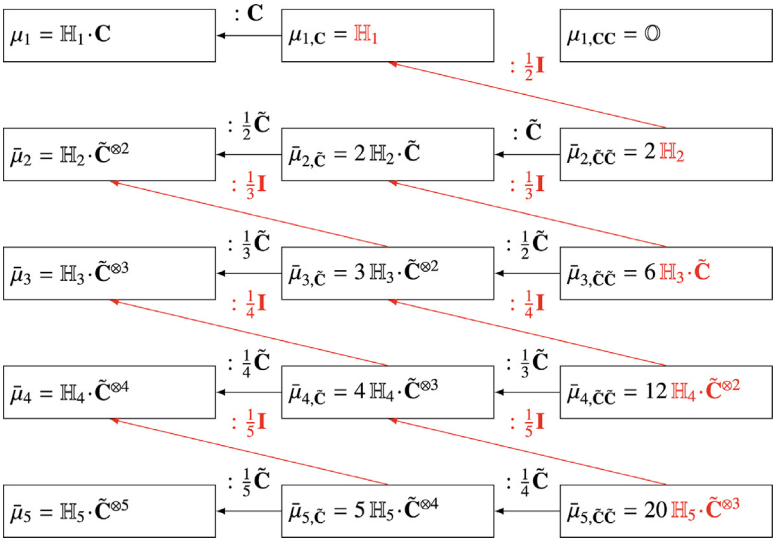

Fig. 2. Efficient computation of the moments and their derivatives starting from the terms marked in red. Details are explained in Section 4.4 in terms of Cartesian components, such that $\mathbb{H}_\alpha \cdot \tilde{\mathbf{C}}^{\otimes\beta} = \mathrm{H}\alpha\mathrm{C}\beta$, where α, β are integers, e.g. $\mathbb{H}_5 \cdot \tilde{\mathbf{C}}^{\otimes 3} = \mathrm{H5C3}$. (For interpretation of the references to colour in this figure legend, the reader is referred to the web version of this article.)

Following the same steps for the higher moments $\bar{\mu}_k = \tilde{C}_{mn}\tilde{C}_{op}\ldots\tilde{C}_{uv}H_{mnop\ldots uv}$ $(k \geq 3)$ one concludes

$$\begin{aligned}\frac{\partial \bar{\mu}_k}{\partial C_{ij}} &= \left(\frac{\partial \tilde{C}_{mn}}{\partial C_{ij}}\tilde{C}_{op}\ldots\tilde{C}_{uv} + \ldots + \tilde{C}_{mn}\tilde{C}_{op}\ldots\frac{\partial \tilde{C}_{uv}}{\partial C_{ij}}\right) H_{mnop\ldots uv} \\ &= k(\delta_{mi}\delta_{nj} - H_{ij}\delta_{mn})\tilde{C}_{op}\ldots\tilde{C}_{uv}H_{mnop\ldots uv} \\ &= k\underbrace{\tilde{C}_{op}\ldots\tilde{C}_{uv}}_{k-1 \text{ copies}}H_{ijop\ldots uv} - kH_{ij}\bar{\mu}_{k-1}\end{aligned} \tag{53}$$

and

$$\begin{aligned}\frac{\partial^2 \bar{\mu}_k}{\partial C_{st}\partial C_{ij}} &= k\left(\frac{\partial \tilde{C}_{op}}{\partial C_{st}}\ldots\tilde{C}_{uv} + \ldots + \tilde{C}_{op}\ldots\frac{\partial \tilde{C}_{uv}}{\partial C_{st}}\right) H_{ijop\ldots uv} - kH_{ij}\frac{\partial \bar{\mu}_{k-1}}{\partial C_{st}} \\ &= k(k-1)(\delta_{os}\delta_{pt} - H_{st}\delta_{op})\cdots\tilde{C}_{uv}H_{ijop\ldots uv} - kH_{ij}\frac{\partial \bar{\mu}_{k-1}}{\partial C_{st}} \\ &= k(k-1)\underbrace{\ldots\tilde{C}_{uv}}_{k-2 \text{ copies}}(H_{ijst\ldots uv} - H_{st}\underbrace{H_{ij\ldots uv}}_{\text{order } 2(k-1)}) - kH_{ij}\frac{\partial \bar{\mu}_{k-1}}{\partial C_{st}}.\end{aligned} \tag{54}$$

4.4. Efficient computation scheme for the moments and their derivatives

The previous sections include all information to compute the moments $\bar{\mu}_k$ and their derivatives. Nevertheless, using the high degree of symmetry of the structural tensors, and in particular the repeated application of the essential property (43), allows defining an efficient scheme to compute the first five moments and their first and second derivatives. The essential steps are illustrated in Fig. 2 and all steps are explained in what follows.

Given components of the five generalised structural tensors

$$H_{ijklmnopqr},\ H_{ijklmnop},\ H_{ijklmn},\ H_{ijkl},\ H_{ij} \tag{55}$$

and the current state of deformation expressed through the components C_{ij} of $\mathbf{C}$, one can calculate

$$\mu_1 = H_{ij}C_{ij}, \quad \tilde{C}_{ij} = C_{ij} - \mu_1\,\delta_{ij}. \tag{56}$$

Next one computes the auxiliary contractions between structural tensors and $\tilde{\mathbf{C}}$

$$\begin{aligned}
\mathrm{H5C3}_{ijkl} &= H_{ijklmnopqr}\tilde{C}_{mn}\tilde{C}_{op}\tilde{C}_{qr},\\
\mathrm{H4C2}_{ijkl} &= H_{ijklmnop}\tilde{C}_{mn}\tilde{C}_{op},\\
\mathrm{H3C1}_{ijkl} &= H_{ijklmn}\tilde{C}_{mn},
\end{aligned} \tag{57}$$

whose further contractions provide

$$\begin{aligned}
\mathrm{H5C4}_{ij} &= \mathrm{H5C3}_{ijkl}\tilde{C}_{kl},\\
\mathrm{H4C3}_{ij} &= \mathrm{H5C3}_{ijkl}\,\delta_{kl},\\
\mathrm{H3C2}_{ij} &= \mathrm{H4C2}_{ijkl}\,\delta_{kl},\\
\mathrm{H2C1}_{ij} &= \mathrm{H3C1}_{ijkl}\,\delta_{kl}.
\end{aligned} \tag{58}$$

The latter can be directly used to compute the affine moments (48) as

$$\begin{aligned}
\bar{\mu}_5 &= \mathrm{H5C4}_{ij}\tilde{C}_{ij},\\
\bar{\mu}_4 &= \mathrm{H5C4}_{ij}\,\delta_{ij},\\
\bar{\mu}_3 &= \mathrm{H4C3}_{ij}\,\delta_{ij},\\
\bar{\mu}_2 &= \mathrm{H3C2}_{ij}\,\delta_{ij},
\end{aligned} \tag{59}$$

as well as their first derivatives

$$\begin{aligned}
(\bar{\mu}_{5,\mathbf{C}})_{ij} &= 5(\mathrm{H5C4}_{ij} - \bar{\mu}_4 H_{ij}),\\
(\bar{\mu}_{4,\mathbf{C}})_{ij} &= 4(\mathrm{H4C3}_{ij} - \bar{\mu}_3 H_{ij}),\\
(\bar{\mu}_{3,\mathbf{C}})_{ij} &= 3(\mathrm{H3C2}_{ij} - \bar{\mu}_2 H_{ij}),\\
(\bar{\mu}_{2,\mathbf{C}})_{ij} &= 2\,\mathrm{H2C1}_{ij},
\end{aligned} \tag{60}$$

and their second derivatives

$$\begin{aligned}
(\bar{\mu}_{5,\mathbf{CC}})_{ijkl} &= 20(\mathrm{H5C3}_{ijkl} - \mathrm{H4C3}_{ij}\,H_{kl} - H_{ij}\,\mathrm{H4C3}_{kl} + \bar{\mu}_3 H_{ij}H_{kl}),\\
(\bar{\mu}_{4,\mathbf{CC}})_{ijkl} &= 12(\mathrm{H4C2}_{ijkl} - \mathrm{H3C2}_{ij}\,H_{kl} - H_{ij}\,\mathrm{H3C2}_{kl} + \bar{\mu}_2 H_{ij}H_{kl}),\\
(\bar{\mu}_{3,\mathbf{CC}})_{ijkl} &= 6(\mathrm{H3C1}_{ijkl} - \mathrm{H2C1}_{ij}\,H_{kl} - H_{ij}\,\mathrm{H2C1}_{kl}),\\
(\bar{\mu}_{2,\mathbf{CC}})_{ijkl} &= 2(H_{ijkl} - H_{ij}H_{kl}).
\end{aligned} \tag{61}$$

For the sake of completeness, we repeat the first results from Section 4.3.

$$(\mu_{1,\mathbf{C}})_{ij} = H_{ij}, \quad (\mu_{1,\mathbf{CC}})_{ijkl} = 0 \tag{62}$$

and emphasise that in all the operations the computational cost can be highly reduced by exploiting the symmetries of the operations arising from symmetries in the generalised structural tensors and $\mathbf{C}$ – for example, of the $3^{10} = 59049$ components of the fifth generalised structural tensor only 66 are unique.

5. Examples and comparisons

The new method for averaging will be applied to two cases inspired by typical problems in biomechanics, and the results will be compared to those obtained by spherical cubature and the Taylor-series based approach, i.e. a higher-order structural tensor method. Particularly, as a representative of the soft collagenous tissue type behaviour we consider an isotropic matrix reinforced by non-linear elastic fibres distributed according to a transversely isotropic orientation density function. Two common approaches, following an additive representation of the matrix and fibre contributions [cf. 40] and the exponential approach according to Rubin and Bodner [41] are considered to define the free energy of the tissue.

5.1. Integration methods

5.1.1. Summary of the proposed approach: 3-point Gauss quadrature

The affinity assumption (35) together with a continuous fibre orientation distribution ensures that the stretch distribution P_Λ is continuous, and hence existence of the density function p_Λ in Eq. (5) for all deformations with

$\bar{\mu}_2 > 0$. Consequently, with the exception of equi-triaxial deformations ($\Lambda_1 = \Lambda_2 = \Lambda_3$) for which $\bar{\mu}_2 = 0$, the Gauss integration can be applied as described in Section 3. The equi-triaxial case is easily treated as an exception (Remark 1) using that in this case $\mathrm{E}[\psi] = \psi(\mu_1)$.

Energy, stress and stiffness are calculated simultaneously according to the scheme described in Section 4.4 (Fig. 2). It is important to note that in the elastic affine case the generalised structural tensors are effectively material parameters, that remain constant during deformation. For this reason, they only need to be computed once for each material, and can hence be stored. As a consequence the potential computational cost of an adequate quadrature rule may be considered of minor importance. Nevertheless, we note that efficient alternative algorithms exist to compute generalised structural tensors for special cases, e.g. those with a single preferred direction leading to transverse isotropy. Hashlamoun and Federico [39].

Algorithm 1 summarises the procedure as a Fortran subroutine-like pseudo code.

function GI (**F**, *mat_param, dist_param*)
- % items to be preserved after return, i.e. reused in subsequent function calls:
- **save** *old_dist_param*
- **save** $\{\mathbb{H}_k\}_{k=1,2,3,4,5}$
- % reuse old or calculate new structural tensors:
- **if** *dist_param* **not** *old_dist_param* **then**
  - compute $\{\mathbb{H}_k\}_{k=1,2,3,4,5}$
  - *old_dist_param* $\leftarrow$ *dist_param*
- **end**
- compute $\mu_1, \{\bar{\mu}_k, \bar{\mu}_{k,\mathbf{C}}, \bar{\mu}_{k,\mathbf{CC}}\}_{k=2,3,4,5}$ (Section 4.4)
- **if** $\bar{\mu}_2 <$ **tol then**
  - $\Psi = \psi(\mu_1)$
  - $\Psi_{,\mathbf{C}} = \psi'(\mu_1)\,\mathbb{H}_1$
  - $\Psi_{,\mathbf{CC}} = \psi''(\mu_1)\,\mathbb{H}_2$
- **else**
  - compute a, b, c, d (23), $\mathcal{I}_1, \mathcal{I}_2, \mathcal{I}_3, \mathcal{A}, \mathcal{B}, \vartheta$ (27), (28), $\{\bar{x}_k\}$ (26)
  - compute $\{x_k\}$ and $\{w_k\}$ (24), (31)
  - compute $\{x_{k,\mathbf{C}}\}$ and $\{w_{k,\mathbf{C}}\}$ (B.1)-(B.7)
  - compute $\{x_{k,\mathbf{CC}}\}$ and $\{w_{k,\mathbf{CC}}\}$ (B.8)-(B.13)
  - $\Psi = \mathrm{GI}[\psi]$ (8)
  - $\Psi_{,\mathbf{C}} = \mathrm{GI}[\psi]_{,\mathbf{C}}$ (32)
  - $\Psi_{,\mathbf{CC}} = \mathrm{GI}[\psi]_{,\mathbf{CC}}$ (33)
- **end**
- $\sigma_{ij} = 2J^{-1}F_{iI}F_{jJ}(\Psi_{,\mathbf{C}})_{IJ}$
- $\mathbb{c}_{ijkl} = 4J^{-1}F_{iI}F_{jJ}F_{kK}F_{lL}(\Psi_{,\mathbf{CC}})_{IJKL}$
- $\tilde{\mathbb{c}}_{ijkl} = \mathbb{c}_{ijkl} + (\sigma_{ik}\delta_{lj} + \sigma_{il}\delta_{kj} + \delta_{ik}\sigma_{lj} + \delta_{il}\sigma_{kj})/2$

return Ψ, σ_{ij}, $\tilde{\mathbb{c}}_{ijkl}$

Algorithm 1: Pseudo code for 3-point Gauss integration of the network free energy, Cauchy stress σ as well as the spatial elasticity tensor $\mathbb{c}$ and the 'Jacobian' $\tilde{\mathbb{c}}$, e.g. for use with continuum elements in Abaqus [42]. For the sake of brevity in notation, Ψ here refers only to the averaged fibre energy, so that $\Psi = \mathrm{E}[\psi]$, i.e. the factor ν_f and additional matrix contributions are omitted. The function takes as input the deformation gradient **F**, material parameters *mat_param* and fibre distribution parameters *dist_param*. Note that, using this function to analyse a series of deformations **F** for a given fibre distribution the structural tensors are only computed once. The inclusion of *dist_param* as an input allows to give a general form that, e.g., provides the typical freedom to analyse different fibre distributions without rewriting code.

5.1.2. Microsphere model for fibre reinforced tissue: Spherical cubature

A discretisation of the unit sphere into a finite set of directions [see e.g. 23], giving rise to what is referred to as microsphere [11,43] or microplane [44,45] model represents the most common strategy to implement affine structural models of soft collagenous tissues with continuous fibre orientation distributions [2,21,46]. In view of the

affine relation (35), the fibre energy $f(\boldsymbol{N}) = \psi(\boldsymbol{N}\cdot\mathbf{C}\boldsymbol{N})$ is accordingly integrated by the cubature rule (7) [see e.g. 43]

$$\mathrm{E}\left[\psi\right] \approx \mathrm{SC}\left[\psi(\boldsymbol{N}\cdot\mathbf{C}\boldsymbol{N})\right] = \sum_{k}^{n} \psi(\boldsymbol{N}_k\cdot\mathbf{C}\boldsymbol{N}_k)\,\rho(\phi_k,\theta_k)\,W_k \tag{63}$$

for integration points $\{\boldsymbol{N}_k\}$, equivalently $\{(\phi_k,\theta_k)\}$, on the unit sphere weighted with $\{W_k\}$. As a consequence of the cubature (63) the derivatives with respect to $\mathbf{C}$ follow as

$$\frac{\partial \mathrm{SC}\left[\psi\right]}{\partial \mathbf{C}} = \sum_{k}^{n} \psi'(\boldsymbol{N}_k\cdot\mathbf{C}\boldsymbol{N}_k)\,\boldsymbol{N}_k\otimes\boldsymbol{N}_k\,\rho(\phi_k,\theta_k)\,W_k \tag{64}$$

and

$$\frac{\partial^2 \mathrm{SC}\left[\psi\right]}{\partial \mathbf{C}\partial \mathbf{C}} = \sum_{k}^{n} \psi''(\boldsymbol{N}_k\cdot\mathbf{C}\boldsymbol{N}_k)\,\boldsymbol{N}_k\otimes\boldsymbol{N}_k\otimes\boldsymbol{N}_k\otimes\boldsymbol{N}_k\,\rho(\phi_k,\theta_k)\,W_k\,. \tag{65}$$

For comparisons with the proposed 1D Gauss integration (Section 5.1.1) the 5810 point Lebedev scheme [27] made available by bur [28] and a 60 point spherical t-design [25,26] has been used, which exactly integrate polynomials in the coordinates x, y, z up to order 131 and 10, respectively. The 5810 point scheme represents a computationally much more expensive ground truth and the 60 point scheme was selected as a typical alternative to the new method.

5.1.3. Generalised higher-order structural tensors: Taylor-series based approach

The higher-order generalised structural tensor approach results from a Taylor expansion of the fibre energy expressed as a function of the affine stretch square stretch (35). Accordingly [cf. 4]

$$\mathrm{E}\left[\psi\right] \approx \mathrm{E}\left[\sum_{k=0}^{n} \frac{1}{k!}\frac{\partial^k \psi}{\partial \Lambda^k}(\Lambda_0)(\Lambda-\Lambda_0)^k\right] = \sum_{k=0}^{n} \frac{1}{k!}\frac{\partial^k \psi}{\partial \Lambda^k}(\Lambda_0)\mathrm{E}\left[(\Lambda-\Lambda_0)^k\right]\,, \tag{66}$$

where $\mathrm{E}\left[(\Lambda-\Lambda_0)^k\right]$ can be identified as the kth moment of the stretch distribution with respect to Λ_0. In view of Eq. (47) (formally replacing μ_1 with Λ_0) this moment can be expressed as

$$\mathrm{E}\left[(\Lambda-\Lambda_0)^k\right] = \underbrace{(C_{ij}-\Lambda_0\delta_{ij})\ldots(C_{mn}-\Lambda_0\delta_{mn})}_{k\ \text{copies}}\,H_{ij\ldots mn}\,. \tag{67}$$

Without additional information that would favour another expansion point, it is reasonable to expand the Taylor series about the point of the expected or mean fibre stretch, i.e. $\Lambda_0 = \mu_1$ [cf. 4,36]. In this case Eq. (67) is the kth central moment and identical to Eq. (67). This choice makes the model consistent with an approach proposed by Cortes and Elliott [47] termed GHOST method, which we will use as a benchmark. The corresponding approximation of the free energy reads

$$\mathrm{E}\left[\psi\right] \approx \mathrm{ST}\left[\psi(\boldsymbol{N}\cdot\mathbf{C}\boldsymbol{N})\right] = \sum_{k=0}^{n} \frac{1}{k!}\frac{\partial^k \psi}{\partial \Lambda^k}(\mu_1)\,\bar{\mu}_k\,, \tag{68}$$

revealing its form as a weighted sum of the central moments (47).

For the sake of completeness, we note that another choice of the expansion point Λ_0 can in some cases improve the approximation qualities of this approach [cf. 4,36], however, generally requires careful consideration of the particular fibre energy function and state of deformation $\mathbf{C}$, and therefore is beyond the scope of this paper.

The derivatives with respect to $\mathbf{C}$ follow as

$$\frac{\partial \mathrm{ST}\left[\psi\right]}{\partial \mathbf{C}} = \sum_{k=0}^{n} \frac{1}{k!}\frac{\partial^{k+1} \psi}{\partial \Lambda^{k+1}}(\mu_1)\,\bar{\mu}_k\,\mathbb{H}_1 + \frac{1}{k!}\frac{\partial^k \psi}{\partial \Lambda^k}(\mu_1)\,\bar{\mu}_{k,\mathbf{C}}\,, \tag{69}$$

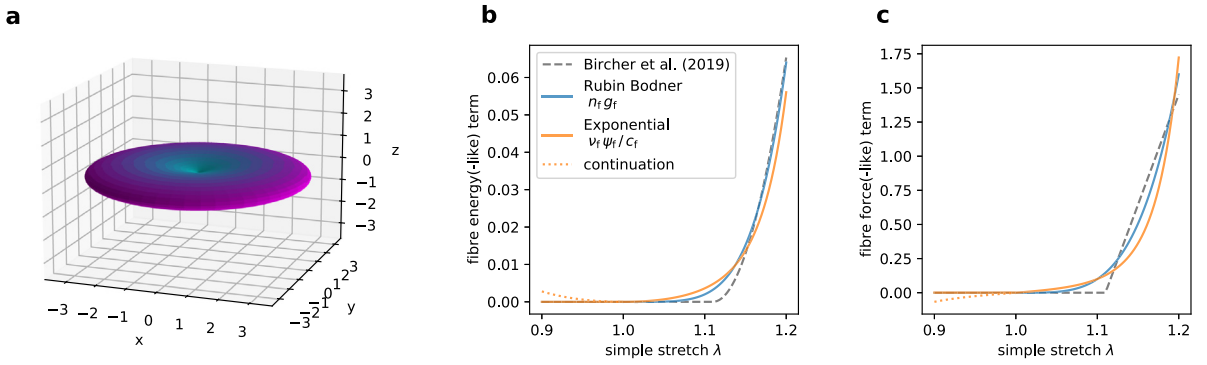

Fig. 3. Fibre material model: (a) Initial fibre orientation distribution density represented as a polar plot. Comparison of (b) energy(-level) and (c) force(-level) terms of the Holzapfel-Gasser-Ogden-type model (72) and Rubin-Bodner-type model (81), as well as the fibre energy used in Bircher et al. [54] that inspired the choice of model parameters (Table 1). In case of the exponential model with tension-compression switch the analytic continuation (without tension-compression switch) is also included for its relevance in the GHOST method.

and

$$\frac{\partial^2 \mathrm{ST}[\psi]}{\partial \mathbf{C} \partial \mathbf{C}} = \sum_{k=0}^{n} \frac{1}{k!} \frac{\partial^{k+2} \psi}{\partial \Lambda^{k+2}}(\mu_1)\, \bar{\mu}_k\, \mathbb{H}_1 \otimes \mathbb{H}_1 + \frac{1}{k!} \frac{\partial^{k+1} \psi}{\partial \Lambda^{k+1}}(\mu_1)\, \bar{\mu}_k\, \mathbb{H}_1 \otimes^s \bar{\mu}_{k,\mathbf{C}} + \frac{1}{k!} \frac{\partial^{k} \psi}{\partial \Lambda^{k}}(\mu_1)\, \bar{\mu}_{k,\mathbf{CC}}\,, \tag{70}$$

where we defined $\otimes^s$ such that $\mathbf{A} \otimes^s \mathbf{B} = \mathbf{A} \otimes \mathbf{B} + \mathbf{B} \otimes \mathbf{A}$ for two arbitrary second order tensors $\mathbf{A}$ and $\mathbf{B}$.

5.2. Specific constitutive assumptions

5.2.1. Anisotropic fibre distribution

As an example of an anisotropic fibre distribution we use a transversely isotropic distribution with respect to a material axes specified by a unit vector $\boldsymbol{N}_0$. The fibre density corresponding to a fibre initial orientation $\boldsymbol{N}(\phi, \theta)$ Eq. (41) is defined through a von Mises distribution [37,48–51] as

$$\rho(\phi, \theta) = K \exp(b(\cos(2\measuredangle(\boldsymbol{N}(\phi, \theta), \boldsymbol{N}_0)) + 1)) = K \exp(2b(\boldsymbol{N}(\phi, \theta) \cdot \boldsymbol{N}_0)^2) \tag{71}$$

with K such that $\mathrm{E}[K] = 1$, i.e. $K = 2\sqrt{2b/\pi}\,/\mathrm{erfi}\sqrt{2b}$ for $b \neq 0$ or otherwise $K = 1$ (continuation), is a normalisation constant (cf. Eq. (6)), b is a concentration parameter and erfi denotes the imaginary error function [49, cf. Remark 4.1 in].

Here, we align the direction $\boldsymbol{N}$ with the unit vector $\boldsymbol{e}_3$ along the z-axis of a Cartesian coordinate system and study the special case $b = -5$, which leads to a transversely isotropic fibre distribution that concentrates fibres in the isotropy plane $(x - y)$, as shown in Fig. 3a. This type of distribution is of particular interest when modelling thin soft tissues and collagenous membranes such as the capsules of organs or the fetal membranes [see e.g. 52,53].

The essential components of the structural tensors required for the GI (Algorithm 1) and ST methods (Section 5.1.3) follow from Eq. (39), (40) and were numerically evaluated for these examples by use of spherical cubature (42). To enforce consistency of the numeric results of the GI method (Algorithm 1), the calculated integration weights $\{\tilde{W}_k\}$ were corrected according to Eq. (44) in Remark 3.

5.2.2. Additive approach for fibre-reinforced materials: Exponential fibre energy

As a first example the exponential fibre energy with tension compression switch is used [cf. 40]

$$\psi = \begin{cases} \frac{c_\mathrm{f}}{2q}(\exp(q(\Lambda - 1)^2) - 1), & \text{if } \Lambda \geq 1, \\ 0, & \text{otherwise}, \end{cases} \tag{72}$$

from which the free energy of the ensemble of reinforcing fibres results as $\Psi_\mathrm{f} = \nu_\mathrm{f}\mathrm{E}[\psi]$ according to Eq. (2). For the complete tissue strain–energy density Ψ the fibre contribution is complemented by an isotropic matrix term Ψ_m so that

$$\Psi = \Psi_\mathrm{m} + \Psi_\mathrm{f}\,, \quad \Psi_\mathrm{f} = \nu_\mathrm{f}\mathrm{E}[\psi]\,, \tag{73}$$

where Ψ_m is chosen as a compressible neo-Hookean material [cf. discussion in 55] with a specific volumetric term found e.g. in Holzapfel [56, Sec. 6.5] and frequently used to account for the compressible matrix in soft tissue [e.g. 52,54]

$$\Psi_\mathrm{m} = \nu_\mathrm{m} c_\mathrm{m} \left(I_1 - 3 + \frac{1}{p}\left(J^{-2p} - 1\right)\right), \quad p > 0\,. \tag{74}$$

From the free energy (72)–(74) the stress and elasticity tensors (1) follow as

$$\mathbf{S} = 2\,\Psi_{\mathrm{m},\mathbf{C}} + 2\nu_\mathrm{f}\mathrm{E}[\psi]_{,\mathbf{C}} \tag{75}$$

and

$$\mathbb{C} = 4\,\Psi_{\mathrm{m},\mathbf{CC}} + 2\nu_\mathrm{f}\mathrm{E}[\psi]_{,\mathbf{CC}}\,, \tag{76}$$

respectively, where $\mathrm{E}[\psi]$ and thus its derivatives may be computed using any of the methods, i.e. GI, SC and ST, explained in Section 5.1. The derivatives of the matrix term read

$$\Psi_{\mathrm{m},\mathbf{C}} = \nu_\mathrm{m} c_\mathrm{m} \left(\frac{1}{3}\,\mathbf{I} - J^{-2p}\,\mathbf{C}^{-1}\right) \tag{77}$$

and

$$\Psi_{\mathrm{m},\mathbf{CC}} = \nu_\mathrm{m} c_\mathrm{m}\, J^{-2p} \left(p\,\mathbf{C}^{-1} \otimes \mathbf{C}^{-1} + \mathbf{C}^{-1} \boxtimes \mathbf{C}^{-1}\right)\,. \tag{78}$$

where '$\boxtimes$' denotes a symmetrising tensor product between second order tensors such that $\mathbf{A}\boxtimes\mathbf{B} : \mathbf{X} = \mathbf{A}(\mathbf{X}+\mathbf{X}^\mathrm{T})\mathbf{B}/2$.

The selection of material parameters will be discussed in Section 5.3 and is specified in Table 1.

5.2.3. Rubin-bodner type model with continuous fibre distribution

In contrast to Eq. (73) the Rubin-Bodner model for fibre reinforced tissue [41] does not consider an additive split between matrix and fibre related energies, even if corresponding terms g_m and g_f, respectively, can be identified. Rubin and Bodner [41] originally proposed a model for tissues reinforced by a discrete number of fibre families and specified their formulation for use with a single family. The model was extended to represent the behaviour of collagenous membranes [57,58] and a continuous representation of statistically distributed fibres was adopted in [53]. The latter form hence considers an averaged contribution of the distributed fibres, which can be understood as the expectation of the fibre contribution $\mathrm{E}[g_\mathrm{f}]$, and hence be computed by means of the Gaussian quadrature proposed in the present work. The correspondingly adapted form of the Rubin-Bodner type strain–energy density of the tissue hence reads

$$\Psi = \frac{c}{2k}\left(\exp\left(k\left(n_\mathrm{m} g_\mathrm{m} + n_\mathrm{f}\mathrm{E}[g_\mathrm{f}]\right)\right) - 1\right), \tag{79}$$

with a matrix term

$$g_\mathrm{m} = I_1 - 3 + \frac{1}{p}\left(J^{-2p} - 1\right), \quad p > 0, \tag{80}$$

similar to Eq. (74) and a fibre related term [41]

$$g_\mathrm{f} = \frac{1}{q}\left\langle \sqrt{\Lambda} - 1\right\rangle^{2q}, \quad q \geq 1, \tag{81}$$

where $\Lambda = \mathbf{C} : \boldsymbol{N}\otimes\boldsymbol{N}$ is the affine stretch, and $\langle\ \rangle$ denote Macaulay brackets. The choice of material parameters k, p, q, n_m, n_f (Table 1) is discussed in Section 5.3.

Based on the free energy (79)–(81) one calculates the stress and elasticity tensors (1) as

$$\mathbf{S} = c\exp\left(k\left(n_\mathrm{m} g_\mathrm{m} + n_\mathrm{f}\mathrm{E}[g_\mathrm{f}]\right)\right)\left(n_\mathrm{m} g_{\mathrm{m},\mathbf{C}} + n_\mathrm{f}\mathrm{E}[g_\mathrm{f}]_{,\mathbf{C}}\right) \tag{82}$$

Table 1
Material parameters of the additive exponential and Rubin-Bodner-type models (Eqs. (73) and (79)): The fibre distribution (71) is specified through $b = -5$ and $\boldsymbol{N}_0 = \boldsymbol{e}_3$.

Model	Parameters							
Add. Exponential			ν_m	c_m [N/mm^2]	ν_f	c_f [N/mm^2]	p	q
			0.88	0.065	0.12	14.97	0.8857	13.48
Rubin-Bodner	c [N/mm^2]	k	n_m		n_f		p	q
	21.5	6.15	5.07e−3		500		0.9	2.5

and

$$\mathbb{C} = c \exp\left(k \left(n_\mathrm{m} g_\mathrm{m} + n_\mathrm{f} \mathrm{E}\left[g_\mathrm{f}\right]\right)\right) \left[2 \left(n_\mathrm{m} g_{\mathrm{m},\boldsymbol{C}} + n_\mathrm{f} \mathrm{E}\left[g_\mathrm{f}\right]_{,\boldsymbol{C}}\right)^{\otimes 2} + \left(n_\mathrm{m} g_{\mathrm{m},\boldsymbol{CC}} + n_\mathrm{f} \mathrm{E}\left[g_\mathrm{f}\right]_{,\boldsymbol{CC}}\right)\right] , \tag{83}$$

where $\mathrm{E}\left[g_\mathrm{f}\right]$ and thus its derivatives may once again be computed by use of any of the methods, i.e. GI, SC and ST, explained in Section 5.1. The derivatives for the matrix term g_m read

$$g_{\mathrm{m},\boldsymbol{C}} = \frac{1}{3} \boldsymbol{I} - J^{-2p} \boldsymbol{C}^{-1} \tag{84}$$

and

$$g_{\mathrm{m},\boldsymbol{CC}} = J^{-2p} \left(p \boldsymbol{C}^{-1} \otimes \boldsymbol{C}^{-1} + \boldsymbol{C}^{-1} \boxtimes \boldsymbol{C}^{-1} \right) . \tag{85}$$

5.3. Choice of model parameters

For the purpose of illustrating the new quadrature scheme, the material parameters of the constitutive models were chosen to be in a range representative for a soft biological tissues (Table 1). To this end we considered the elastic response reported by Bircher et al. [54] for bovine Glisson's capsule, a thin collagenous tissue surrounding the liver.

For the Rubin-Bodner model (Section 5.2.3) we largely adopted the model parameters calibrated in Bircher et al. [54, Eq. 1] for bovine Glisson's capsule (Table 1), specified for a membrane with thickness of 0.1 mm. The parameters were interpreted to match with our formulation (79), and the constants n_f and q were refitted as illustrated in Fig. 3b, c to omit the use of an additional fibre slackness parameter introduced in [54].

The model parameters of the exponential fibre law (Section 5.2.2) were tuned to provide a similar overall response as for the Rubin-Bodner type model when applied to the loadcases considered in Section 5.5 (cf. Figs. 4 and 5). Notably, the two different model formulations lead to a different response in terms of the individual matrix and fibre contributions as well as the tissue (cf. discussion in Stracuzzi et al. [53]). The fibre behaviour of both parametrised models is illustrated in Fig. 3b, c in a scaled representation. This behaviour is extracted from the stretch dependent fibre energy term in the exponential fibre model $\nu_\mathrm{f} \psi_\mathrm{f}$ and the corresponding fibre 'energy level' term in the Rubin-Bodner-type model $n_\mathrm{f} g_\mathrm{f}$. In addition to the fibre 'energy level' behaviour shown in Fig. 3b, c represents the fibre 'force level' behaviour, defined as the derivative of the former with respect to the fibre stretch $\lambda = \sqrt{\Lambda}$.

The fibre distribution for both models (Eqs. (73) and (79)) is chosen such that it reflects transverse isotropy with respect to the thickness direction of the thin tissue and strong fibre alignment in the isotropy plane, and is prescribed by Eq. (71) with $b = -5$ (Fig. 3a). We note that in [54] these characteristics were captured by distributing a finite number of fibres in the membrane plane which displayed slight alternating up and down off-plane inclinations instead of a continuous representation.

5.4. Numerical implementation

The Gauss integration and benchmark methods for both the exponential fibre model and Rubin-Bodner type model were implemented as subroutines in Fortran, available for download at [59]. These subroutines were either called from Python scripts (Python 3.7.3) after compilation with help of the numpy.f2py module, or from a Abaqus/Standard (v6.14-1) User Subroutine [60].

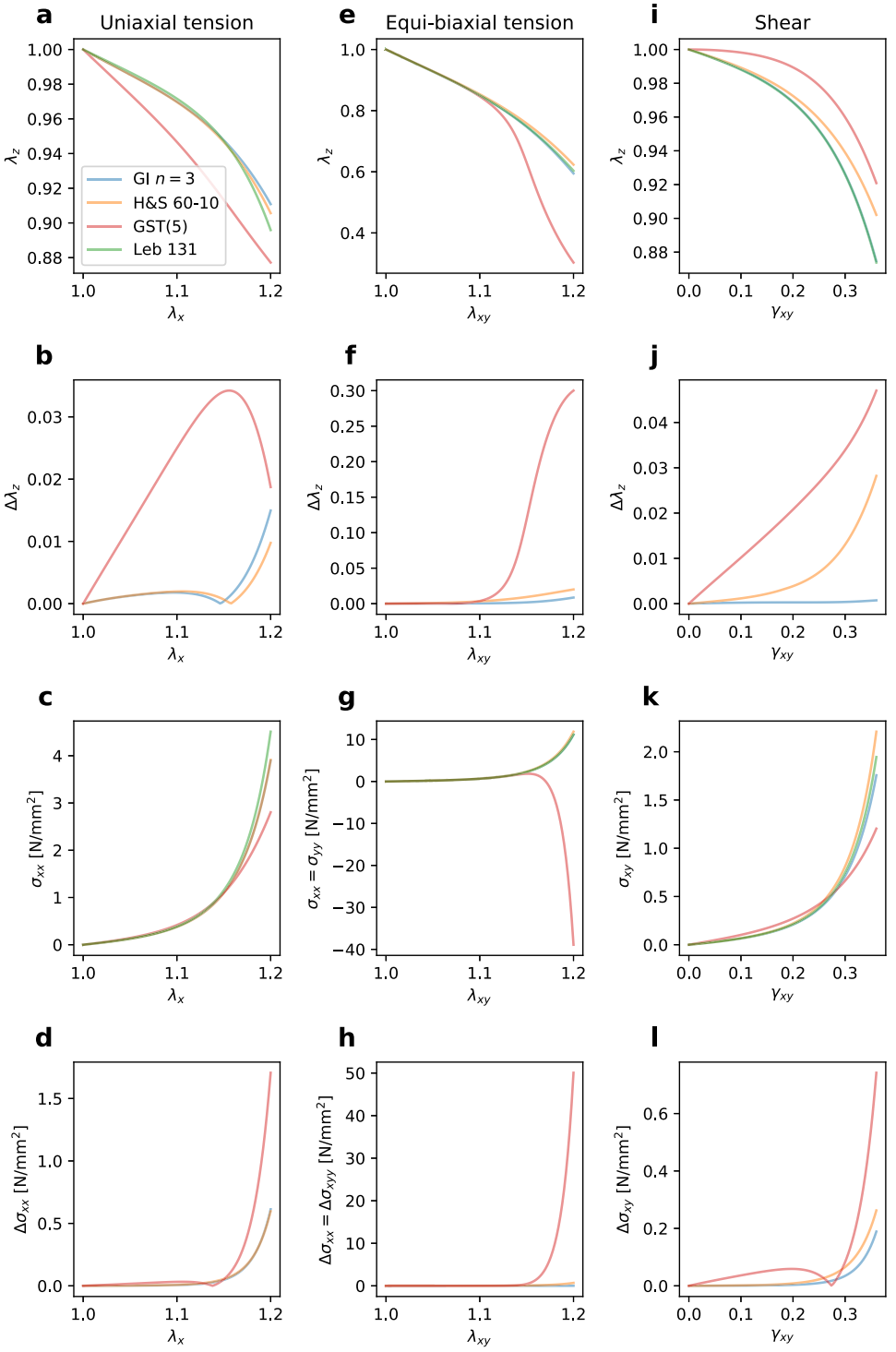

Fig. 4. Additive exponential model: Comparison between H&S 60-10 rule, 5th order GST approach and 1D 3-point Gauss rule. The fibre distribution parameters are $\boldsymbol{N}_0 = \boldsymbol{e}_3$ and $b = -5$. In case of the GST approach the switch of the fibre energy is neglected and the analytic continuation of the fibre energy is used for stretches smaller 1.

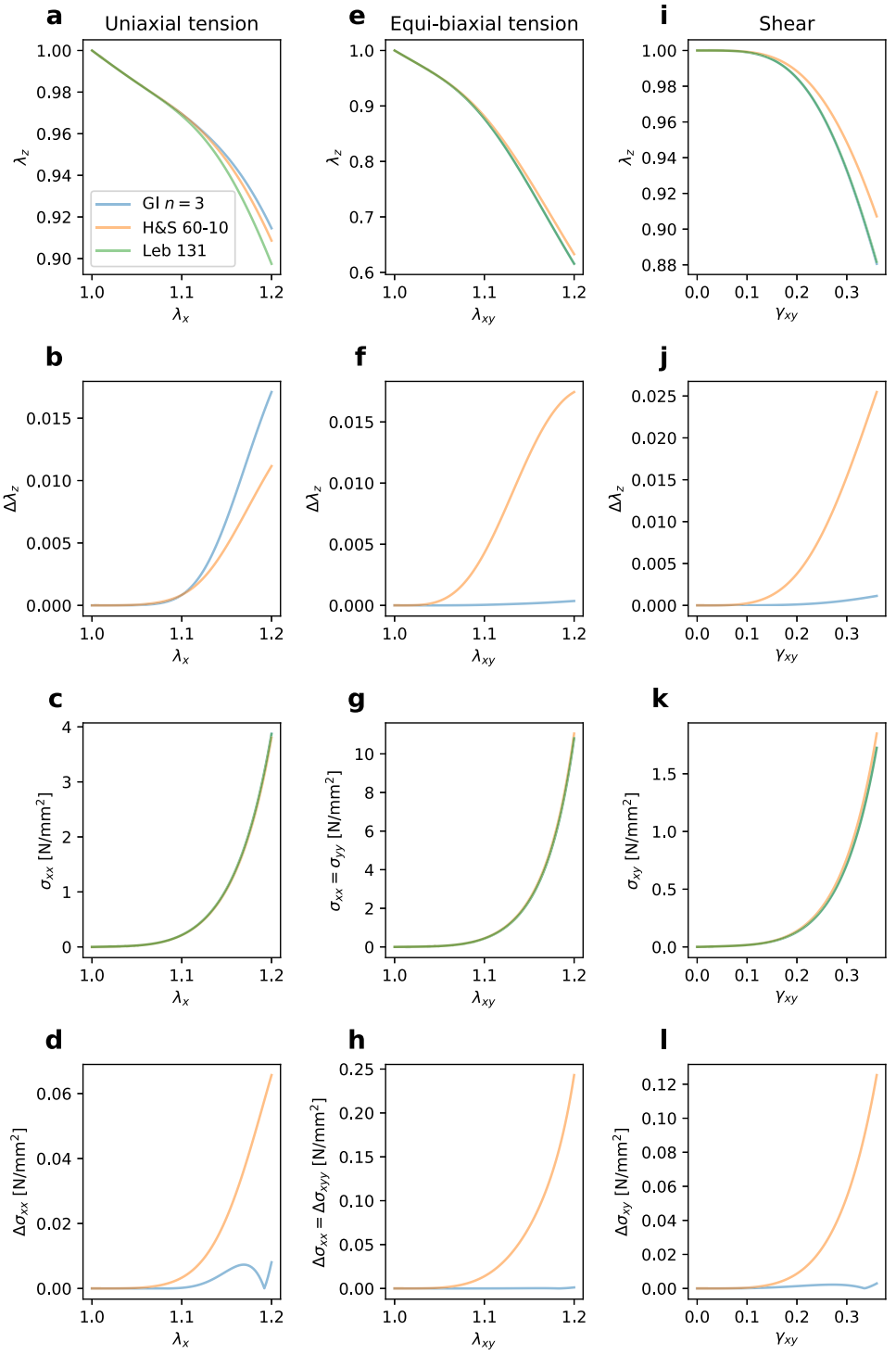

Fig. 5. Rubin-Bodner-type model: Comparison between H&S 60–10 rule and 1D 3-point Gauss rule. The fibre distribution parameters are $N_0 = \boldsymbol{e}_3$ and $b = -5$.

The responses computed by the different methods when applied to analyse some simple homogeneous deformation states by means of Python scripts were used to study the accuracy of the methods and to showcase the beneficial

property of the proposed method with regard to the issue of induced anisotropy. Finite element simulations with Abaqus/Standard (v6.14-1) were further used to analyse and illustrate the models' performance in an academic example.

5.5. Analysis of computational accuracy

To illustrate the general computational accuracy of the 3-point Gauss integration in comparison with the selected benchmark methods, we consider uniaxial extension within the membrane plane with lateral contraction, described by

$$\mathbf{F}_{\mathrm{UA}} = \lambda_x \boldsymbol{e}_1 \otimes \boldsymbol{e}_1 + \lambda_y \boldsymbol{e}_2 \otimes \boldsymbol{e}_2 + \lambda_z \boldsymbol{e}_3 \otimes \boldsymbol{e}_3 \,. \tag{86}$$

The tensile stretch λ_x is prescribed, while λ_y, λ_z are determined such that the strain–energy density is minimised, implying traction-free lateral directions. Equibiaxial extension within the membrane plane was considered through

$$\mathbf{F}_{\mathrm{EB}} = \lambda_{xy} \boldsymbol{e}_1 \otimes \boldsymbol{e}_1 + \lambda_{xy} \boldsymbol{e}_2 \otimes \boldsymbol{e}_2 + \lambda_z \boldsymbol{e}_3 \otimes \boldsymbol{e}_3 \,, \tag{87}$$

where λ_{xy} was prescribed, while λ_z was computed such that the strain–energy density was at a minimum (which implied a stress-free state in z direction). Noteworthy, for anisotropic materials, these pure homogeneous deformation states correspond to simple and equibiaxial tension only in special cases, viz. if the directions $\boldsymbol{e}_x$, $\boldsymbol{e}_y$, $\boldsymbol{e}_z$ coincide with principal axes of material symmetry. Given that the stretch is applied in the isotropy plane $(x - y)$, this holds for the GI and ST method by definition. The slight anisotropy induced by the position of the integration points of the SC method, however, might generally violate this condition, depending on the symmetry of the integration scheme.

In addition, a shear type deformation

$$\mathbf{F}_{\mathrm{SH}} = \boldsymbol{e}_1 \otimes \boldsymbol{e}_1 + \gamma_{xy} \boldsymbol{e}_1 \otimes \boldsymbol{e}_2 + \boldsymbol{e}_2 \otimes \boldsymbol{e}_2 + \lambda_z \boldsymbol{e}_3 \otimes \boldsymbol{e}_3 \tag{88}$$

was studied, in which the direction perpendicular to the shear plane was assumed to be free of normal stress, i.e. γ_{xy} is prescribed, while λ_z is optimised to minimise energy.

Energy minimisation to compute the unknown stretches was performed by applying the Nelder–Mead simplex algorithm implemented in the Python function scipy.optimize.minimize to the energy output of the Fortran subroutine.

It has been discussed that the Taylor-series based generalised higher order structural tensor method can lead to discontinuities in the response when applied to piece-wise defined fibre free energies [4,61–63]. More precisely, in the generalised 5th order structural tensor approach the fibre energy function should be analytic or at least 5 times continuously differentiable [cf. 4]. As a consequence this method cannot be applied in a straightforward manner to any of the investigated fibre energy functions with tension-compression switch. For the exponential fibre energy we therefore substituted Eq. (72) by the version without switch (see analytic continuation in Fig. 3) as previously proposed [37,47]. Since for the Rubin-Bodner fibre energy (81) there is no analytic continuation (because of q being real valued), the method was omitted in this case.

Figs. 4 and 5, respectively, display the simulation results for both constitutive models in terms of the computed stretches (λ_z), its deviation ($\Delta\lambda_z$) from the numeric ground truth, the tensile or shear stress (σ_{xx}, σ_{xy}), and the corresponding differences ($\Delta\sigma_{xx}, \Delta\sigma_{xy}$). Inspection of these results reveals that only in terms of the predicted lateral stretches in the uniaxial extension test, the new method with 3 integration points (GI $n = 3$) is slightly less accurate than the 10th order spherical cubature with 60 points. In all other cases it yields either comparable results or outperforms the spherical 10-design.

Fig. 4 also shows that the results of the 5th order generalised structural tensor approach without fibre switch (GST(5)) leads to much larger errors.

5.6. Analysis of induced anisotropy

It was noted previously in literature that the directions specified through the set of integration points of spherical cubature schemes can interfere with the material symmetry prescribed by the orientation distribution function [43,64]. This problem is particularly evident in allegedly isotropic materials with uniformly distributed fibres, in which the effect of the integration scheme becomes visible as induced anisotropy [see the discussions in 17,65–67].

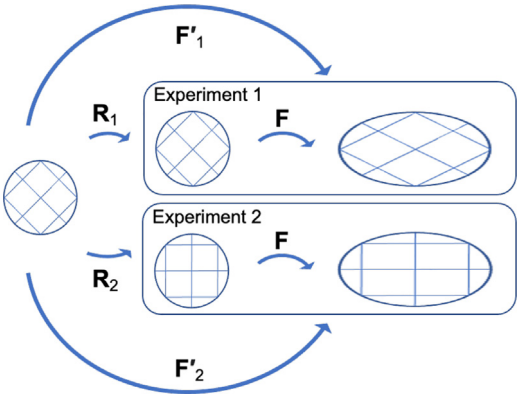

Fig. 6. Illustration of the test performed to analyse induced anisotropy. The pattern has been added to guide the eye.

To illustrate that the new method is not affected by this problem, we applied rotations $\mathbf{R}$ prior to subjecting the material with properties described in Section 5.2 to a homogeneous state of deformation given by $\mathbf{F}$, so that the overall deformation state was expressed by

$$\mathbf{F}' = \mathbf{F}\mathbf{R} \tag{89}$$

[cf. 17]. This procedure is illustrated in Fig. 6 for the case of two such experiments, where the pattern has been added to guide the eye.

Particularly the response was studied for

$$\mathbf{F} = 1.2\boldsymbol{e}_1\otimes\boldsymbol{e}_1 + 0.7\boldsymbol{e}_2\otimes\boldsymbol{e}_2 + 0.4\boldsymbol{e}_3\otimes\boldsymbol{e}_3\,. \tag{90}$$

$\mathbf{R}$ was chosen to represent a rotation by an angle φ about either the $\boldsymbol{e}_3$ axis (aligned with z) or the $\boldsymbol{e}_2$ axis (aligned with y), so that

$$\mathbf{R}_A = \cos(\varphi)\,(\boldsymbol{e}_1\otimes\boldsymbol{e}_1 + \boldsymbol{e}_B\otimes\boldsymbol{e}_B) + \sin(\varphi)\,(\boldsymbol{e}_1\otimes\boldsymbol{e}_B - \boldsymbol{e}_B\otimes\boldsymbol{e}_1) + \boldsymbol{e}_A\otimes\boldsymbol{e}_A \;\text{ (no sum)}, \tag{91}$$

where either $A = 3$, $B = 2$, or $A = 2$, $B = 3$. Given the perfect symmetry of the material models within the x, y-plane, ideally the first case ($\mathbf{R}_3$) should not affect the results while the second case ($\mathbf{R}_2$) should capture the transverse isotropy defined through the von Mises orientation distribution function (71). We generated $\mathbf{F}'$ as described above for 100 equidistant angles $\varphi \in [0, 2\pi)$. For all such $\mathbf{F}'$, both material models and each integration method (see Section 5.1), we computed the corresponding stress based on Fortran routines called from Python scripts. The results are presented in terms of the value of the first principal stress depending on the rotation angle φ in Fig. 7.

Figs. 7a, b reveal the obvious anisotropy induced by the 60 point spherical 10-design, which per definition is not present in the Gauss integration or generalised structural tensor approaches. As already observed in the accuracy tests in Section 5.5 the H&S 60–10 and the GI $n=3$ method have different computational errors, here observed as different distances of the orange and blue curves from the green dotted ground truth. Interestingly, in Figs. 7a and b the computational error of the GI $n=3$ method is throughout smaller than the varying deviation due to the induced anisotropy of the H&S 60–10 scheme. On the other hand, despite errors in accuracy, all schemes thoroughly capture the anisotropy induced through the strong preferred alignment of the fibres towards the $\boldsymbol{e}_3$ material axis (Fig. 7c, d).

5.7. Finite element example

Calling the Fortran subroutines available at [59] within the Abaqus UMAT subroutine [cf. 60, Sec. 1.1.14] the code for the Gauss quadrature and benchmark methods can directly be used in finite element simulations with Abaqus/Standard.

This is showcased in a finite element example that was inspired by the investigations in Bircher et al. [54], and exemplifies a 0.1 mm thick membrane sample of 100 mm × 100 mm with a central circular defect of 2 mm

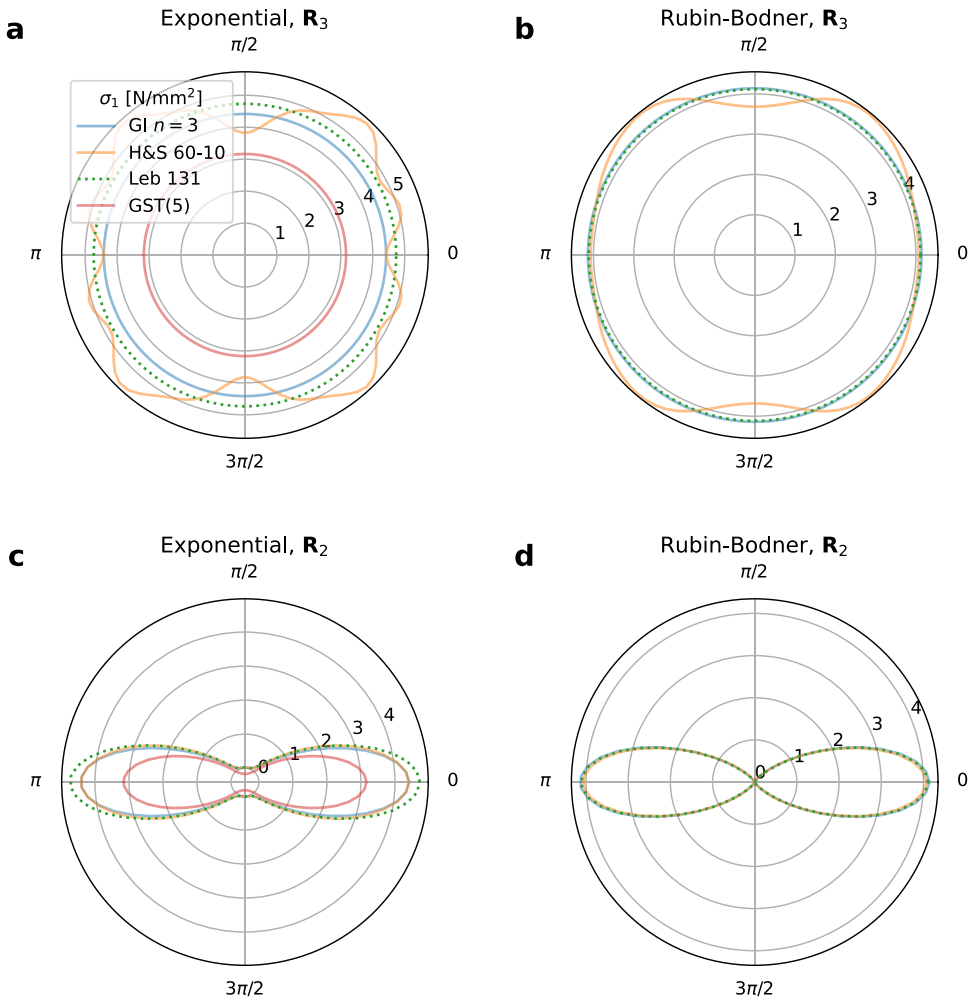

Fig. 7. Induced anisotropy. 1st principal Cauchy stress σ_1 of two transversely isotropic materials (cf. Table 1) obtained when imposing deformations $\mathbf{F}' = \mathbf{F}\mathbf{R}$ with $\mathbf{F}$ according to (90), and $\mathbf{R}$ representing either (a, b) a rotation about the axis of symmetry ($\mathbf{R}_3$) or (c, d) about an axis within the isotropy plane ($\mathbf{R}_2$).

diameter in the centre. For reasons of symmetry only one eighth of this sample was modelled in Abaqus and discretised by quadratic hexahedral elements with reduced integration (C3D20R). To mimic the effect of a planar equibiaxial extension, the free lateral faces of the model were displaced by 20% of their length, corresponding to an equibiaxial stretch of 1.2 in a membrane without defect (Fig. 8).

The finite element simulations were run with both the additive exponential and Rubin-Bodner-type model equipped with the parameters reported in Table 1, and results were generated for both the 3-point Gauss integration (GI $n = 3$) and the spherical 10-design (SC H&S 60–10).

The results are shown in Fig. 9, in terms of radial stress with respect to a cylindrical coordinate system whose z-axis coincides with the membrane normal, and we anticipate that the corresponding contour plot should display perfect radial symmetry. In line with the results in Sections 5.5 and 5.6 one can observe that while the overall range of the results displays only minor differences due to the different numeric approach, the spherical 10-design leads to deviations from radial symmetry as a clear indicator of the effect of induced anisotropy.

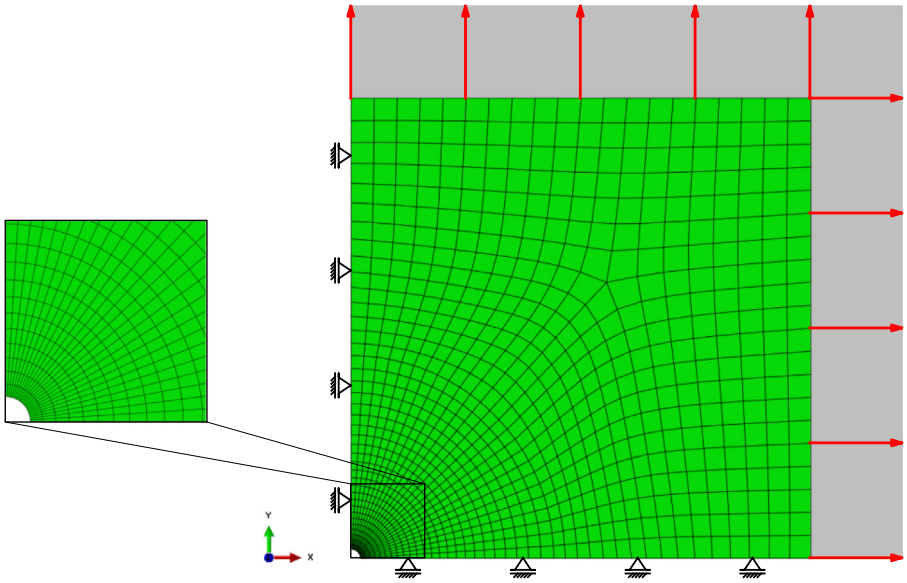

Fig. 8. Illustration of the finite element example of a thin sheet of tissue with central circular defect, subject to equibiaxial extension at its boundaries.

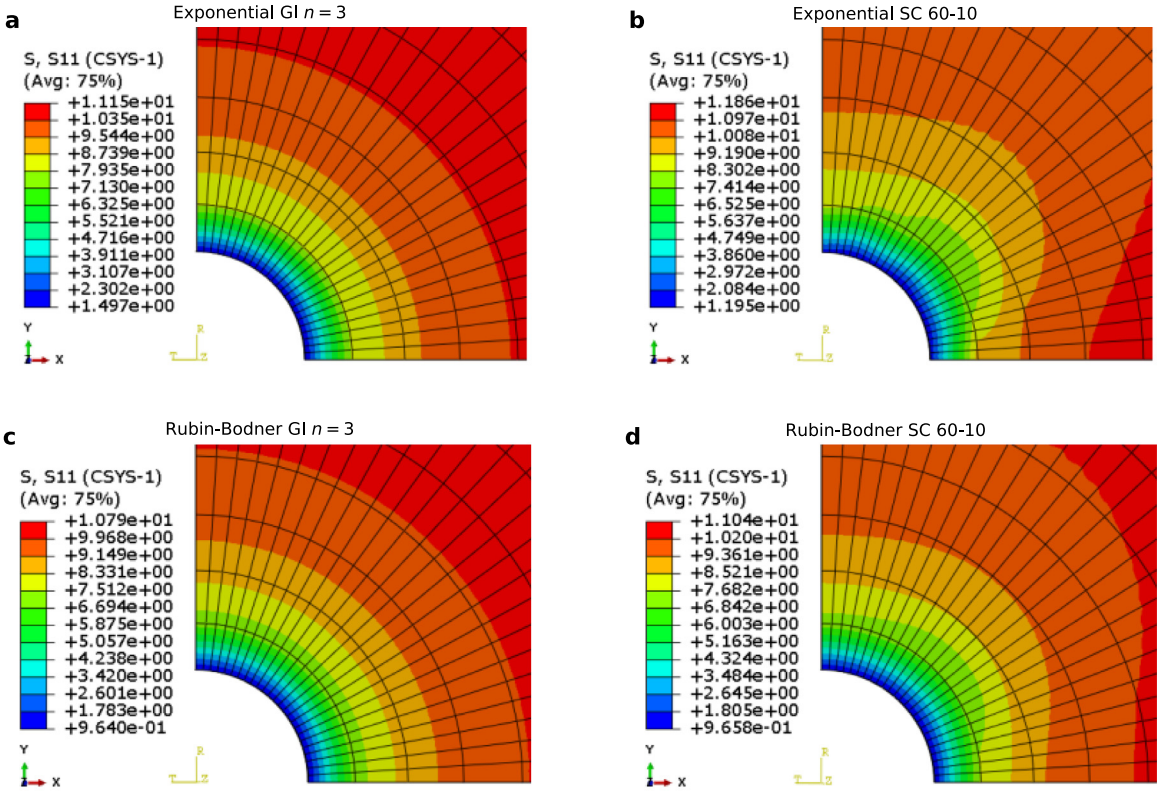

Fig. 9. Abaqus simulations: Comparison between integrations using 3-point Gauss rule (left) and 60-point spherical 10-design (right). The upper and lower pair of images correspond to the additive exponential (73) and Rubin-Bodner-type fibre laws (79), respectively. The radial component of the Cauchy stress (S11 in MPa) is shown.

5.8. A note on computational costs

To obtain a rough estimate of how the computational cost compares between the methods in Section 5.1, the response of the models in Sections 5.2.2 and 5.2.3 to 10, 000 random homogeneous states of deformation, viz.

$$\mathbf{F} = \mathbf{R}\mathbf{Q}\left(\lambda_1\, \boldsymbol{e}_1\otimes\boldsymbol{e}_1 + \lambda_2\, \boldsymbol{e}_2\otimes\boldsymbol{e}_2 + \lambda_3\, \boldsymbol{e}_3\otimes\boldsymbol{e}_3\right)\mathbf{Q}^{\mathrm{T}} \tag{92}$$

for random principal stretches $\{\lambda_i\}$ between 0.1 and 2 and rotation tensors $\mathbf{R}$ and $\mathbf{Q}$ was determined with the different methods executed under comparable conditions (e.g. same machine). The computational cost of the implementations of the spherical 60-design and 3-point Gauss integration as well as the 5th higher order generalised structural tensor approach were found to be virtually indistinguishable, while the cost of the 5810-point Lebedev integration was roughly 2.5 and 4.5 higher for the models in Eqs. (73) and (79), respectively.

6. Discussion

We have proposed a new method to evaluate the strain–energy density function and constitutive relations of soft tissues and materials with distributed fibres according to the structural approach, i.e. by integrating the free energy of single fibres with orientational statistics governed by an orientation density function. The new method is based on univariate Gauss quadrature of the fibre free energy expressed in terms of the squared fibre stretch, i.e. a real scalar variable. The applicability of the well-known Gauss type approximation of the integral is a consequence of transforming the integral over distributed fibres on the unit sphere into an integral over the stretch distribution on the domain of positive reals, as recently developed in [4,18].

6.1. Applicability

If the orientation distribution is uniform, the method generally applies to any case in which the statistical moments of the distribution of square stretch can be expressed in terms of the macroscopic deformation. For non-uniform orientation distributions discussed in the present work, the existence of a relation $\Lambda_{\boldsymbol{N}} : \boldsymbol{N} \mapsto \Lambda$ is required between the referential direction of a fibre and its (square) stretch that it experiences due to a macroscopic deformation $\mathbf{F}$. Based on such a relation, the stretch distribution and its moments may be obtained by variable transformations [4,34,35]. The affine modelling approach, where $\Lambda_{\boldsymbol{N}} = (\mathbf{F}\boldsymbol{N})^2$ clearly falls into this category and has a wide range of applications. This case is elaborated in the present paper, thus providing an alternative approach to the discretised microsphere models [23,43–45,64] or methods based on a Taylor series expansion of the fibre energy [36,37], such as the GHOST method [47], for the implementation of affine structrual models [2,21,46].

6.2. Properties

Compared to the latter two existing methods the univariate Gaussian integration neither impairs the material symmetry defined by the orientation distribution as it is known for classical cubature on the sphere [17,65–67], nor does its quality of approximation strongly suffer from non-analytic integrands, e.g. caused by fibre switches that set the free energy zero when the fibre undergoes compression, which currently limits the application of the Taylor series approaches [see the discussions in 61–63].

Even for cases where the integrand is well-behaved Gauss integration may be favoured over approaches based upon a Taylor expansion of the integrand since it does not require the choice of an expansion point to guarantee convergence [36]. Furthermore, the method only requires the integrand and not its derivatives to be evaluated at the Gauss points, whereas the use of a m-order Taylor expansion of the fibre energy, requires the evaluation of additional m derivatives that can be computationally costly to evaluate at each of these levels.

Several advantages of the new method result from the separated integration of the fibre constitutive law and the orientation distribution function, which in the classical methods are integrated as a product. In the here presented approach, the fibre law alone is evaluated in the Gaussian quadrature rule with n integration points $\{x_k\}$, and hence is exact for polynomials of order $2n-1$ that match with the fibre constitutive function at these n locations. The orientation distribution function, on the other hand, only affects the positions of $\{x_k\}$ and the values of the weights $\{w_k\}$. If the referential fibre orientation is non-uniform, the anisotropy is considered through the $2n-1$ even order generalised structural tensors up to tensorial order $2(2n-1)$. Like in Taylor series approaches [37], they can be

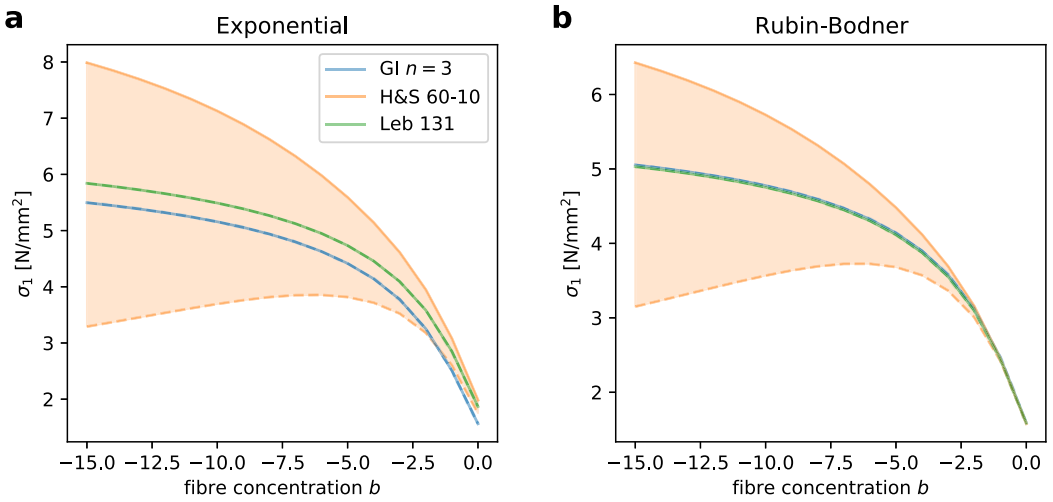

Fig. 10. Induced anisotropy depends on non-uniformity of orientation distribution: Smallest (dashed) and largest (solid) value of the 1st principal Cauchy stress σ_1 for two transversely isotropic materials (cf. Table 1) with concentration parameter b, obtained when imposing deformations $\mathbf{F}' = \mathbf{FR}$ with $\mathbf{F}$ according to (90), and $\mathbf{R}$ representing a rotation about the axis of symmetry ($\mathbf{R}_3$).

calculated by spherical cubature at arbitrarily high order, i.e very high accuracy. The non-linearity of the orientation distribution does thus not impair the quality by which the fibre energy is integrated. This undesired effect is vice-versa well-known for spherical cubature with fixed integration points on the sphere since the non-linearity of the integrand – the product of orientation density and fibre energy – changes both with stretch and orientation, while the integration points remain at their original position on the sphere. We note that non-linear mappings of the integration points have been proposed to address this problem [64,68], are however not commonly used.

In order to illustrate the beneficial effect of separating the non-linearity of the fibre law from the non-uniformity of the orientation distribution, we repeat the analyses conducted in Section 5.6 for various values of the fibre dispersion parameter b, ranging from 0 (isotropy) to -15 (strong alignment within the isotropy plane). For each b, the smallest and largest value of the maximum principal stress σ_1 obtained upon rotating the deformation state (90) about the axis $\boldsymbol{e}_3$ in 100 steps according to Eq. (89) was recorded, and is plotted in Fig. 10. While for the GI method, just like for an ideal ground truth, the maximal principal stress takes a unique value for each b, it is observed that the range of values (shaded area) predicted for spherical cubature increases with increasing anisotropy, i.e. $|b|$. The extent of the fibre orientation's non-uniformity hence affects the accuracy of the spherical cubature, in clear contrast to the here proposed GI method.

As already observed for $b = -5$ in Fig. 7, the GI result nearly coincides with the ground truth (Leb 131) for the Rubin-Bodner type model (Fig. 10b) for all b studied, while it has a small offset for the additive energy formulation with exponential fibre law (Fig. 10a).

The numerical example in Fig. 10a allows for another interesting observation: There might be cases – in fact those with close-to-uniform fibre orientation distributions so that $|b|$ is small – where the spherical 10-design (H&S 60–10) performs better than the GI method, here roughly for $-2 < b < 0$, while with increasing anisotropy, GI is closer to the ground truth.

Another advantage of the separation between the integration of orientation distribution and fibre energy results from the fact that the orientation distribution density is typically considered constant in time for elastic materials, so that the structural tensors need to be computed only once in a boundary value problem. After that, their components represent constant material parameters that can be stored and reused, so that only the Gaussian integration of the fibre energy needs to be accomplished in each step.

6.3. Effective use of information at integration points

The n integration points for Gaussian integration are given by the n roots of the nth orthogonal polynomials, and since particularly compact analytical solutions exist for the roots of polynomials with $n \leq 3$, we have analysed

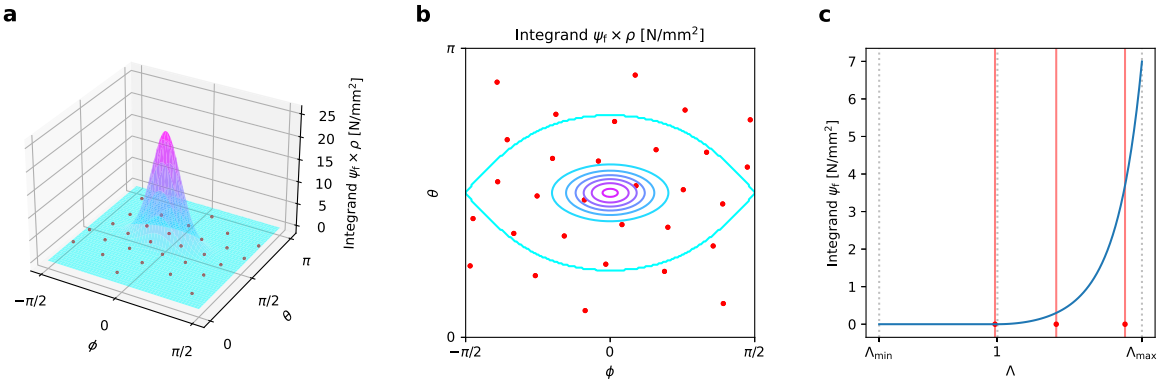

Fig. 11. Illustration of the functions to be integrated for the determination of $\mathrm{E}[\psi_\mathrm{f}]$ in spherical cubature as a landscape (a) and contour plot (b), and with Gauss quadrature (c). Both examples represent the identical material (ψ_f and ρ given by Eq. (72), (71)) and state of deformation, given by $\mathbf{F} = 1.2\boldsymbol{e}_1 \otimes \boldsymbol{e}_1 + 1\boldsymbol{e}_2 \otimes \boldsymbol{e}_2 + 0.8\boldsymbol{e}_3 \otimes \boldsymbol{e}_3$. The red points indicate the positions of the integration points (60 and 3). Due to symmetry of the problem only the range $\phi \in [-\pi/2, \pi/2]$, including only 30 of the 60 spherical integration points is shown. (For interpretation of the references to colour in this figure legend, the reader is referred to the web version of this article.)

the 3-point quadrature in more detail. We have found that already at this low order the method can compete with typical spherical integration (a spherical 10-design), and even outperform the latter in either dealing with piecewise defined, non-smooth integrands or in the quality by which material symmetry is preserved. The fact that such high accuracy can be achieved with only 3 integration points may seems surprising and is (i) due to the separation of the deformation dependent terms from the orientation distribution, so that the Gauss rule evaluated at these 3 points only need to integrate the fibre constitutive law, and (ii) because of the optimal choice of these locations in the (square) stretch domain. The latter point is illustrated in Fig. 11, that shows for the same material and state of deformation the integrand in spherical integration (a, b) and the one used for Gauss integration (c) together with the corresponding integration points, at which this integrand is evaluated. It is clearly observed in this example, that a majority of the points used for spherical cubature (here defined by the particular 10-design) lie in regions where the function to be integrated is fairly linear while they lack in the non-linear region. This problem is due to the orientation distribution multiplying the fibre energy and thus strongly biasing the integrand. In contrast, the 3 points in (c) are optimal in the sense that they exactly integrate any polynomial of order 5 that matches the fibre energy in these three points. Loosely speaking, the accuracy of this method depends on how well the fibre strain–energy density function is captured by a 5th order polynomial within the domain of interest, which in the affine case is spanned by the values of the minimal and maximal principal square stretch. As mentioned above the method is therefore correct for any fibre energy that is a polynomial of square stretch of order $n \leq 5$. We emphasise again that this property does generally not hold for the spherical t-design even with $t = 10$: The latter integrates exactly *spherical polynomials* up to order 10, but the corresponding order of the integrand is determined by the product $\rho(\phi, \theta)\psi(\lambda)$, which for the typically used distribution functions is not a spherical polynomial at all, even if ψ is.

6.4. Computational cost and current limitations

In the dedicated test application that was considered, our implementation of the 3-point Gauss quadrature and other existing approaches with reasonable choices of spherical integration points and Taylor series terms, demonstrated comparable computational efficiency such that their computation times could not be distinguished. However, these times strongly depend on the specific problem, for example the considered material behaviour, state of deformation and the finite element model. For methods using higher-order structural tensors the computational time is strongly affected by the reusability of their once computed components [cf. the discussion in 47].

We emphasise that in cases where the referential orientation density changes, as it occurs e.g. in models that take into account growth and remodelling [69], the structural tensors need to be recomputed so that the computational effort increases.

Finally, compared to the quite ubiquitous spherical cubature, which is able to approximately integrate any, even inelastic, type of fibre constitutive equation without major changes of the concept, the new method in its present

form has been developed for the hyperelastic case thus far. Although we do explicitly not exclude applicability of the method to more general fibre behaviour, this case was not discussed here, and needs thoughtful consideration in future work.

7. Conclusions

In this study, we have presented a univariate Gauss quadrature rule for integrating the fibre strain-energy, as well as stress and stiffness, in materials with generally non-uniform fibre distributions such as soft collagenous tissues. The method is thus suitable to compute the averaged tissue properties according to the structural approach. i.e. when fibre properties are averaged over an orientation distribution defined in the reference configuration.

The obtained quadrature rules do not induce spurious additional anisotropy and are robust in case of piece-wise defined fibre strain–energy density functions resulting e.g. when neglecting the contribution of 'compressed' fibres. In these aspects, already the special case with $n = 3$ integration points elaborated in the present work performs better than the typical alternatives of spherical cubature and Taylor-expansion of the integrand, while associated with comparable numerical cost.

The beneficial properties of the method are mainly due to an intrinsic separation of the averaging operation into a deformation-dependent integral over the fibre stretch distribution, and a deformation-independent integral over the fibre orientation distribution that leads to higher-order structural tensors. The efficiency, in particular, comes from the reusability of the latter once they have been computed, similar to other generalised structural tensor approaches.

Given that the structural approach and conceptionally similar models are widespread, we believe that the new method has great potential for a wide range of problems even beyond applications in soft tissue biomechanics.

Funding

This work was supported by the Swiss National Science Foundation (SNSF, Grant No. 182014).

Declaration of competing interest

The authors declare that they have no known competing financial interests or personal relationships that could have appeared to influence the work reported in this paper.

Data availability

No data was used for the research described in the article

Appendix A. Basic proofs

In this section we present common proofs for three essential properties of the Gauss quadrature: (i) the n-point rule integrates polynomials up to degree $2n-1$ exactly, (ii) the weights $\{w_i\}$ are all positive, (iii) the integration points are real, distinct and lie within the integration interval, i.e. $[\Lambda_{\min}, \Lambda_{\max}]$ [cf. e.g. 29].

Proof (*Property (i)*)**.** The factorised representation of the nth orthogonal polynomial is

$$P_n(x) = \prod_{i=1}^{n}(x - x_i), \quad x_1 < x_2 < \ldots < x_n. \tag{A.1}$$

Let the function $f(x)$ be a polynomial of degree $\leq 2n-1$ that we want to integrate. The Lagrange interpolation of this function using the interpolation points $\{x_i\}$ is

$$g(x) = \sum_{i=1}^{n} f(x_i) \prod_{\substack{j=1 \\ j\neq i}}^{n} \frac{x - x_j}{x_i - x_j}\,. \tag{A.2}$$

Since $f(x) - g(x)$ is a polynomial of degree $\leq 2n-1$ that satisfies $f(x) - g(x) = 0$ at $x = x_j$ for $j = 1, 2, \ldots, n$, one can write

$$f(x) - g(x) = d(x) P_n(x)\,, \tag{A.3}$$

where $d(x)$ is a polynomial of degree $\leq n-1$. Consequently making use of the linearity of the integral and the characteristic orthogonality of P_n to all polynomials of lower degree, i.e. $\mathrm{E}\left[d(x)P_n(x)\right]=0$, the integral of $f(x)$ is

$$\mathrm{E}\left[f(x)\right]=\mathrm{E}\left[g(x)+d(x)P_n(x)\right]=\mathrm{E}\left[g(x)\right]=\sum_{i=1}^{n} f(x_i)\underbrace{\mathrm{E}\left[\prod_{\substack{j=1\\ j\neq i}}^{n}\frac{x-x_j}{x_i-x_j}\right]}_{=w_i}, \tag{A.4}$$

which, as the right hand side is the n-point Gauss quadrature rule, proves claim (i). □

Proof (*Property (ii)*)**.** Let us define the polynomial of degree $n-1$

$$\omega_{n,i}(x)=\prod_{\substack{j=1\\ j\neq i}}^{n}\frac{x-x_j}{x_i-x_j} \tag{A.5}$$

with the essential property $w_i=\mathrm{E}\left[\omega_{n,i}(x)\right]$. Since $\omega_{n,i}(x)=0$ at $x=x_j$ for all $j=1\ldots,n$ except $j=i$ for which it is 1, one can deduce that $\omega_{n,i}^2(x)-\omega_{n_i}(x)=0$ at $x=x_j$ for all $j=1,2,\ldots,n$ and thus

$$\omega_{n,i}^2(x)-\omega_{n_i}(x)=q(x)P_n(x)\,, \tag{A.6}$$

where $q(x)$ is a polynomial of degree $n-2$. Hence one has

$$\mathrm{E}\left[\omega_{n,i}^2(x)-\omega_{n_i}(x)\right]=\mathrm{E}\left[q(x)P_n(x)\right]=0\,, \tag{A.7}$$

because of the orthogonality $P_n\perp q(x)$. The claim (ii) follows by linearity of the integral, viz.

$$w_i=\mathrm{E}\left[\omega_{n,i}(x)\right]=\mathrm{E}\left[\omega_{n_i}^2(x)\right]>0\,. \quad \square \tag{A.8}$$

Proof (*Property (iii)*)**.** Let us again consider the factorised form of the nth orthogonal polynomial

$$P_n(z)=\prod_{j=1}^{n}(z-z_j)\,. \tag{A.9}$$

Let us now separate any hypothetical complex roots, which according to the fundamental theorem of algebra occur in complex conjugated pairs and real roots inside and outside the interval $\mathcal{I}=[\Lambda_{\min},\Lambda_{\max}]$, i.e. roots within $\mathcal{I}$ and $\mathbb{R}\backslash\mathcal{I}$, viz.

$$P_n(x)=\prod_{\{z_j\in\mathcal{I}\}}(z-z_j)\prod_{\{z_k\in\mathbb{R}\backslash\mathcal{I}\}}(z-z_k)\prod_{\substack{\text{complex pairs}\\ \{x\pm iy\}}}\left((z-x)^2+y^2\right). \tag{A.10}$$

Here one can see that the product term associated with the complex pairs of roots and real roots outside $\mathcal{I}$ do not change sign for $z\in\mathcal{I}$. By multiplying $P_n(x)$ with $(z-z_l)$ for each real root z_l in $\mathcal{I}$ with an odd multiplicity m_{z_l}, the resulting expression remains sign-consistent over $\mathcal{I}$, and hence integrating this expression will necessarily produce a non-zero value, viz.

$$\mathrm{E}\left[P_n(x)\prod_{\{z_l\in\mathcal{I}:m_{z_l}\,\mathrm{odd}\}}(z-z_l)\right]\neq 0\,. \tag{A.11}$$

Because of the orthogonality of P_n to all polynomials of degree $\leq n-1$, this implies $\prod_{\{z_l\in\mathcal{I}:m_{z_l}\,\mathrm{odd}\}}(z-z_l)$ must be a polynomial of degree n, meaning there must be n real roots in $\mathcal{I}$ with multiplicity 1, which proves claim (iii). □

Appendix B. Derivatives for 3-point rule

We here provide the expressions to obtain the first derivatives of the integration points $\{x_k\}$ and weights $\{w_k\}$ in analytic forms. The former follow from

$$\begin{aligned}
a_{,\mathbf{C}} &= (\bar{\mu}_4 - 3\bar{\mu}_2^2)\bar{\mu}_{2,\mathbf{C}} - 2\bar{\mu}_3\bar{\mu}_{3,\mathbf{C}} + \bar{\mu}_2\bar{\mu}_{4,\mathbf{C}}\,,\\
b_{,\mathbf{C}} &= (2\bar{\mu}_2\bar{\mu}_3 - \bar{\mu}_5)\bar{\mu}_{2,\mathbf{C}} + (\bar{\mu}_2^2 + \bar{\mu}_4)\bar{\mu}_{3,\mathbf{C}} + \bar{\mu}_3\bar{\mu}_{4,\mathbf{C}} - \bar{\mu}_2\bar{\mu}_{5,\mathbf{C}}\,,\\
c_{,\mathbf{C}} &= (2\bar{\mu}_2\bar{\mu}_4 - \bar{\mu}_3^2)\bar{\mu}_{2,\mathbf{C}} + (\bar{\mu}_5 - 2\bar{\mu}_2\bar{\mu}_3)\bar{\mu}_{3,\mathbf{C}} + (\bar{\mu}_2^2 - 2\bar{\mu}_4)\bar{\mu}_{4,\mathbf{C}} + \bar{\mu}_3\bar{\mu}_{5,\mathbf{C}}\,,\\
d_{,\mathbf{C}} &= (2\bar{\mu}_2\bar{\mu}_5 - \bar{\mu}_3\bar{\mu}_4)\bar{\mu}_{2,\mathbf{C}} + (3\bar{\mu}_3^2 - 2\bar{\mu}_2\bar{\mu}_4)\bar{\mu}_{3,\mathbf{C}} - 2\bar{\mu}_2\bar{\mu}_3\bar{\mu}_{4,\mathbf{C}} + \bar{\mu}_2^2\bar{\mu}_{5,\mathbf{C}}\,,
\end{aligned} \tag{B.1}$$

$$\mathcal{I}_{1,\mathbf{C}} = -\frac{\mathcal{I}_1 a_{,\mathbf{C}} + b_{,\mathbf{C}}}{a}, \quad \mathcal{I}_{2,\mathbf{C}} = \frac{c_{,\mathbf{C}} - \mathcal{I}_2 a_{,\mathbf{C}}}{a}, \quad \mathcal{I}_{3,\mathbf{C}} = -\frac{\mathcal{I}_3 a_{,\mathbf{C}} + d_{,\mathbf{C}}}{a}, \tag{B.2}$$

$$\mathcal{A}_{,\mathbf{C}} = 2\mathcal{I}_1\mathcal{I}_{1,\mathbf{C}} - 3\mathcal{I}_{2,\mathbf{C}}, \quad \mathcal{B}_{,\mathbf{C}} = \left(3\mathcal{I}_1^2 - \frac{9}{2}\right)\mathcal{I}_{1,\mathbf{C}} - \frac{9}{2}\mathcal{I}_1\mathcal{I}_{2,\mathbf{C}} + \frac{27}{2}\mathcal{I}_{3,\mathbf{C}}, \tag{B.3}$$

$$\vartheta_{,\mathbf{C}} = \frac{1}{\sqrt{\mathcal{A}^3 - \mathcal{B}^2}}\left(\frac{3}{2}\frac{\mathcal{B}}{\mathcal{A}}\mathcal{A}_{,\mathbf{C}} - \mathcal{B}_{,\mathbf{C}}\right), \tag{B.4}$$

so that

$$\boxed{\bar{x}_{k,\mathbf{C}} = \frac{1}{3}\mathcal{I}_{1,\mathbf{C}} + \frac{1}{3}C_k\mathcal{A}^{-1/2}\mathcal{A}_{,\mathbf{C}} - \frac{2}{9}\mathcal{A}^{1/2}S_k\vartheta_{,\mathbf{C}}, \quad x_{k,\mathbf{C}} = \mathbb{H}_1 + \bar{x}_{k,\mathbf{C}}}\,, \tag{B.5}$$

and the latter are obtained as

$$v_{k,\mathbf{C}} = (3\bar{x}_k - \mathcal{I}_1)\,\bar{x}_{k,\mathbf{C}} - (\bar{x}_k - \bar{x}_j)\,\bar{x}_{l,\mathbf{C}} - (\bar{x}_k - \bar{x}_l)\,\bar{x}_{j,\mathbf{C}}\,, \tag{B.6}$$

$$\boxed{w_{k,\mathbf{C}} = \frac{1}{v_k}\left(\bar{\mu}_{2,\mathbf{C}} + \bar{x}_j\bar{x}_{l,\mathbf{C}} + \bar{x}_l\bar{x}_{j,\mathbf{C}} - w_k v_{k,\mathbf{C}}\right)}\,. \tag{B.7}$$

The second derivatives follow accordingly by calculating

$$\begin{aligned}
a_{,\mathbf{CC}} &= (\bar{\mu}_4 - 3\bar{\mu}_2^2)\bar{\mu}_{2,\mathbf{CC}} - 2\bar{\mu}_3\bar{\mu}_{3,\mathbf{CC}} + \bar{\mu}_2\bar{\mu}_{4,\mathbf{CC}}\\
&\quad + \bar{\mu}_{2,\mathbf{C}} \otimes^s \bar{\mu}_{4,\mathbf{C}} - 6\bar{\mu}_2\bar{\mu}_{2,\mathbf{C}}^{\otimes 2} - 2\bar{\mu}_{3,\mathbf{C}}^{\otimes 2}\,,\\
b_{,\mathbf{CC}} &= (2\bar{\mu}_2\bar{\mu}_3 - \bar{\mu}_5)\bar{\mu}_{2,\mathbf{CC}} + (\bar{\mu}_2^2 + \bar{\mu}_4)\bar{\mu}_{3,\mathbf{CC}} + \bar{\mu}_3\bar{\mu}_{4,\mathbf{CC}} - \bar{\mu}_2\bar{\mu}_{5,\mathbf{CC}}\\
&\quad + 2\bar{\mu}_3\bar{\mu}_{2,\mathbf{C}}^{\otimes 2} + 2\bar{\mu}_2\bar{\mu}_{2,\mathbf{C}} \otimes^s \bar{\mu}_{3,\mathbf{C}} - \bar{\mu}_{2,\mathbf{C}} \otimes^s \bar{\mu}_{5,\mathbf{C}} + \bar{\mu}_{3,\mathbf{C}} \otimes^s \bar{\mu}_{4,\mathbf{C}}\,,\\
c_{,\mathbf{CC}} &= (2\bar{\mu}_2\bar{\mu}_4 - \bar{\mu}_3^2)\bar{\mu}_{2,\mathbf{CC}} + (\bar{\mu}_5 - 2\bar{\mu}_2\bar{\mu}_3)\bar{\mu}_{3,\mathbf{CC}} + (\bar{\mu}_2^2 - 2\bar{\mu}_4)\bar{\mu}_{4,\mathbf{CC}} + \bar{\mu}_3\bar{\mu}_{5,\mathbf{CC}}\\
&\quad + 2\bar{\mu}_4\bar{\mu}_{2,\mathbf{C}}^{\otimes 2} + 2\bar{\mu}_2\bar{\mu}_{2,\mathbf{C}} \otimes^s \bar{\mu}_{4,\mathbf{C}} - 2\bar{\mu}_3\bar{\mu}_{2,\mathbf{C}} \otimes^s \bar{\mu}_{3,\mathbf{C}} + \bar{\mu}_{3,\mathbf{C}} \otimes^s \bar{\mu}_{5,\mathbf{C}}\\
&\quad - 2\bar{\mu}_2\bar{\mu}_{3,\mathbf{C}}^{\otimes 2} - 2\bar{\mu}_{4,\mathbf{C}}^{\otimes 2}\,,\\
d_{,\mathbf{CC}} &= (2\bar{\mu}_2\bar{\mu}_5 - \bar{\mu}_3\bar{\mu}_4)\bar{\mu}_{2,\mathbf{CC}} + (3\bar{\mu}_3^2 - 2\bar{\mu}_2\bar{\mu}_4)\bar{\mu}_{3,\mathbf{CC}} - 2\bar{\mu}_2\bar{\mu}_3\bar{\mu}_{4,\mathbf{CC}} + \bar{\mu}_2^2\bar{\mu}_{5,\mathbf{CC}}\\
&\quad + 2\bar{\mu}_5\bar{\mu}_{2,\mathbf{C}}^{\otimes 2} + 2\bar{\mu}_2\bar{\mu}_{2,\mathbf{C}} \otimes^s \bar{\mu}_{5,\mathbf{C}} - 2\bar{\mu}_4\bar{\mu}_{2,\mathbf{C}} \otimes^s \bar{\mu}_{3,\mathbf{C}} - 2\bar{\mu}_3\bar{\mu}_{2,\mathbf{C}} \otimes^s \bar{\mu}_{4,\mathbf{C}}\\
&\quad + 6\bar{\mu}_3\bar{\mu}_{3,\mathbf{C}}^{\otimes 2}\,,
\end{aligned} \tag{B.8}$$

where here and henceforth the notations $\mathbf{A}^{\otimes 2} = \mathbf{A} \otimes \mathbf{A}$ and $\mathbf{A} \otimes^s \mathbf{B} = \mathbf{A} \otimes \mathbf{B} + \mathbf{B} \otimes \mathbf{A}$ are used for any pair of second order tensors $\mathbf{A}$ and $\mathbf{B}$. One proceeds with

$$\begin{aligned}
\mathcal{I}_{1,\mathbf{CC}} &= -\frac{1}{a}\left(b_{,\mathbf{CC}} + a_{,\mathbf{C}} \otimes^s \mathcal{I}_{1,\mathbf{C}} + \mathcal{I}_1 a_{,\mathbf{CC}}\right)\,,\\
\mathcal{I}_{2,\mathbf{CC}} &= \frac{1}{a}\left(c_{,\mathbf{CC}} - a_{,\mathbf{C}} \otimes^s \mathcal{I}_{2,\mathbf{C}} - \mathcal{I}_2 a_{,\mathbf{CC}}\right)\,,\\
\mathcal{I}_{2,\mathbf{CC}} &= -\frac{1}{a}\left(d_{,\mathbf{CC}} + a_{,\mathbf{C}} \otimes^s \mathcal{I}_{3,\mathbf{C}} - \mathcal{I}_3 a_{,\mathbf{CC}}\right)\,,
\end{aligned} \tag{B.9}$$

so that

$$\begin{aligned}
\mathcal{A}_{,\mathbf{CC}} &= 2\mathcal{I}_1\mathcal{I}_{1,\mathbf{CC}} - 3\mathcal{I}_{2,\mathbf{CC}} + 2\mathcal{I}_{1,\mathbf{C}}^{\otimes 2}\,,\\
\mathcal{B}_{,\mathbf{CC}} &= \left(3\mathcal{I}_1^2 - \frac{9}{2}\right)\mathcal{I}_{1,\mathbf{CC}} - \frac{9}{2}\mathcal{I}_1\mathcal{I}_{2,\mathbf{CC}} + \frac{27}{2}\mathcal{I}_{3,\mathbf{CC}} + 6\mathcal{I}_1\mathcal{I}_{1,\mathbf{C}}^{\otimes 2} - \frac{9}{2}\mathcal{I}_{1,\mathbf{C}} \otimes^s \mathcal{I}_{2,\mathbf{C}}\,,
\end{aligned} \tag{B.10}$$

$$\begin{aligned}
\vartheta_{,\mathbf{CC}} &= (\mathcal{A}^3 - \mathcal{B}^2)^{-3/2}\left[\left(\frac{3}{2}\frac{\mathcal{B}^2}{\mathcal{A}^2} - 15\mathcal{A}\right)\mathcal{B}\mathcal{A}_{,\mathbf{C}}^{\otimes 2} + \frac{3}{2}\mathcal{A}^2\mathcal{A}_{,\mathbf{C}} \otimes^s \mathcal{B}_{,\mathbf{C}} - \mathcal{B}\mathcal{B}_{,\mathbf{C}}^{\otimes 2}\right]\\
&\quad + (\mathcal{A}^3 - \mathcal{B}^2)^{-1/2}\left(\frac{3}{2}\frac{\mathcal{B}}{\mathcal{A}}\mathcal{A}_{,\mathbf{CC}} - \mathcal{B}_{,\mathbf{CC}}\right),
\end{aligned} \tag{B.11}$$

and finally

$$\begin{aligned}
x_{k,\mathbf{CC}} = \bar{x}_{k,\mathbf{CC}} = {} & \frac{1}{3}\mathcal{I}_{1,\mathbf{CC}} + \frac{1}{3}C_k\mathcal{A}^{-1/2}\mathcal{A}_{,\mathbf{CC}} - \frac{2}{9}\mathcal{A}^{1/2}S_k\vartheta_{,\mathbf{CC}}\\
& - \frac{1}{9}S_k\mathcal{A}^{-1/2}\mathcal{A}_{,\mathbf{C}} \otimes^s \vartheta_{,\mathbf{C}}\\
& - \frac{1}{6}C_k\mathcal{A}^{-3/2}\mathcal{A}_{,\mathbf{C}}^{\otimes 2} - \frac{2}{27}\mathcal{A}^{-1/2}C_k\vartheta_{,\mathbf{C}}^{\otimes 2}
\end{aligned} \tag{B.12}$$

and

$$\begin{aligned}
w_{k,\mathbf{CC}} = \frac{1}{v_k}\Big(& \bar{\mu}_{2,\mathbf{CC}} - w_k\left[(3\bar{x}_k - \mathcal{I}_1)\bar{x}_{k,\mathbf{CC}} + 4\bar{x}_{k,\mathbf{C}}^{\otimes 2} - \bar{x}_{k,\mathbf{C}} \otimes^s \mathcal{I}_{1,\mathbf{C}}\right]\\
& - w_{k,\mathbf{C}} \otimes^s v_{k,\mathbf{C}}\\
& + \left[\bar{x}_j + w_k(\bar{x}_k - \bar{x}_j)\right]\bar{x}_{l,\mathbf{CC}} + \left[\bar{x}_l + w_k(\bar{x}_k - \bar{x}_l)\right]\bar{x}_{j,\mathbf{CC}}\\
& + (1 - w_k)\bar{x}_{j,\mathbf{C}} \otimes^s \bar{x}_{l,\mathbf{C}}\Big)
\end{aligned}. \tag{B.13}$$

References

[1] M.S. Sacks, Incorporation of experimentally-derived fiber orientation into a structural constitutive model for planar collagenous tissues, J. Biomech. Eng. 125 (2) (2003) 280–287, http://dx.doi.org/10.1115/1.1544508.

[2] Y. Lanir, A structural theory for the homogeneous biaxial stress-strain relationships in flat collagenous tissues, J. Biomech. 12 (6) (1979) 423–436, http://dx.doi.org/10.1016/0021-9290(79)90027-7.

[3] W. Freeden, M. Gutting, Integration and Cubature Methods: A Geomathematically Oriented Course, Chapman and Hall/CRC, 2017, http://dx.doi.org/10.1201/9781315195674.

[4] B.R. Britt, A.E. Ehret, Constitutive modelling of fibre networks with stretch distributions, Part II: Alternative representation, affine distribution and anisotropy, J. Mech. Phys. Solids 175 (2023) 105291, http://dx.doi.org/10.1016/j.jmps.2023.105291.

[5] P.L. Chandran, V.H. Barocas, Affine versus non-affine fibril kinematics in collagen networks: theoretical studies of network behavior, J. Biomech. Eng. 128 (2) (2006) 259–270, http://dx.doi.org/10.1115/1.2165699.

[6] E.A. Sander, T. Stylianopoulos, R.T. Tranquillo, V.H. Barocas, Image-based multiscale modeling predicts tissue-level and network-level fiber reorganization in stretched cell-compacted collagen gels, Proc. Natl. Acad. Sci. 106 (42) (2009) 17675–17680, http://dx.doi.org/10.1073/pnas.0903716106.

[7] A. Mauri, R. Hopf, A.E. Ehret, C.R. Picu, E. Mazza, A discrete network model to represent the deformation behavior of human amnion, J. Mech. Behav. Biomed. Mater. 58 (2016) 45–56, http://dx.doi.org/10.1016/j.jmbbm.2015.11.009.

[8] S. Domaschke, M. Zündel, E. Mazza, A.E. Ehret, A 3D computational model of electrospun networks and its application to inform a reduced modelling approach, Int. J. Solids Struct. 158 (2019) 76–89, http://dx.doi.org/10.1016/j.ijsolstr.2018.08.030.

[9] M. Puso, Mechanistic Constitutive Models for Rubber Elasticity and Viscoelasticity, Technical Report UCRL-ID-151578, Lawrence Livermore National Lab., CA (US), 2003, http://dx.doi.org/10.2172/15004918.

[10] M.F. Beatty, An average-stretch full-network model for rubber elasticity, J. Elasticity 70 (1) (2003) 65–86, http://dx.doi.org/10.1023/B:ELAS.0000005553.38563.91.

[11] C. Miehe, S. Göktepe, F. Lulei, A micro-macro approach to rubber-like materials—Part I: The non-affine micro-sphere model of rubber elasticity, J. Mech. Phys. Solids 52 (2004) 2617–2660, http://dx.doi.org/10.1016/j.jmps.2004.03.011.

[12] M. Tkachuk, C. Linder, The maximal advance path constraint for the homogenization of materials with random network microstructure, Phil. Mag. 92 (22) (2012) 2779–2808, http://dx.doi.org/10.1080/14786435.2012.675090.

[13] A. Raina, C. Linder, A homogenization approach for nonwoven materials based on fiber undulations and reorientation, J. Mech. Phys. Solids 65 (2014) 12–34, http://dx.doi.org/10.1016/j.jmps.2013.12.011.

[14] P.J. Hunter, Myocardial constitutive laws for continuum mechanics models of the heart, in: S. Sideman, R. Beyar (Eds.), Molecular and Subcellular Cardiology: Effects of Structure and Function, in: Advances in Experimental Medicine and Biology, Springer US, Boston, MA, 1995, pp. 303–318, http://dx.doi.org/10.1007/978-1-4615-1893-8_30.

[15] C.O. Horgan, G. Saccomandi, A description of arterial wall mechanics using limiting chain extensibility constitutive models, Biomech. Model. Mechanobiol. 1 (4) (2003) 251–266, http://dx.doi.org/10.1007/s10237-002-0022-z.
[16] G.A. Holzapfel, R.W. Ogden, On the tension–compression switch in soft fibrous solids, Eur. J. Mech. A Solids 49 (2015) 561–569, http://dx.doi.org/10.1016/j.euromechsol.2014.09.005.
[17] A.E. Ehret, M. Itskov, H. Schmid, Numerical integration on the sphere and its effect on the material symmetry of constitutive equations—A comparative study, Internat. J. Numer. Methods Engrg. 81 (2) (2010) 189–206, http://dx.doi.org/10.1002/nme.2688.
[18] B.R. Britt, A.E. Ehret, Constitutive modelling of fibre networks with stretch distributions. Part I: Theory and illustration, J. Mech. Phys. Solids 167 (2022) 104960, http://dx.doi.org/10.1016/j.jmps.2022.104960.
[19] W. Gautschi, On generating Gaussian quadrature rules, in: G. Hämmerlin (Ed.), Numerische Integration, series=International Series of Numerical Mathematics / Internationale Schriftenreihe zur Numerischen Mathematik / Série Internationale D'Analyse Numérique, Vol. 45, Birkhäuser, Basel, 1979, pp. 147–154, http://dx.doi.org/10.1007/978-3-0348-6288-2_10.
[20] Y. Lanir, Constitutive equations for fibrous connective tissues, J. Biomech. 16 (1) (1983) 1–12, http://dx.doi.org/10.1016/0021-9290(83)90041-6.
[21] K.L. Billiar, M.S. Sacks, Biaxial mechanical properties of the native and glutaraldehyde-treated aortic valve cusp: Part II–A structural constitutive model, J. Biomech. Eng. 122 (4) (2000) 327–335, http://dx.doi.org/10.1115/1.1287158.
[22] Y. Lanir, Multi-scale structural modeling of soft tissues mechanics and mechanobiology, J. Elasticity 129 (1) (2017) 7–48, http://dx.doi.org/10.1007/s10659-016-9607-0.
[23] P. Bažant, B.H. Oh, Efficient numerical integration on the surface of a sphere, ZAMM Z. Angew. Math. Mech. 66 (1) (1986) 37–49, http://dx.doi.org/10.1002/zamm.19860660108.
[24] P.-B. Badel, J.-B. Leblond, A note on integration schemes for the microplane model of the mechanical behaviour of concrete, Commun. Numer. Methods. Eng. 20 (1) (2004) 75–81, http://dx.doi.org/10.1002/cnm.658.
[25] R.H. Hardin, N.J.A. Sloane, McLaren's improved snub cube and other new spherical designs in three dimensions, Discrete Comput. Geom. 15 (4) (1996) 429–441, http://dx.doi.org/10.1007/BF02711518.
[26] Hardin, R.H. and Sloane, N.J.A., Spherical Designs (2002), http://neilsloane.com/sphdesigns/, [Accessed: 2022-11-24].
[27] V.I. Lebedev, Quadratures on a sphere, USSR Comput. Math. Math. Phys. 16 (2) (1976) 10–24, http://dx.doi.org/10.1016/0041-5553(76)90100-2.
[28] J. Burkardt, Sphere Lebedev Rule – Quadrature Rules for the Sphere (2010), https://people.sc.fsu.edu/~jburkardt/datasets/sphere_lebedev_rule/sphere_lebedev_rule.html, [Accessed: 2022-11-24].
[29] J. Stoer, R. Bulirsch, Introduction to Numerical Analysis, third ed., Springer, 2002.
[30] M. Abramowitz, I.A. Stegun, Handbook of Mathematical Functions with Formulas, Graphs, and Mathematical Tables, U S Department of Commerce, 1972.
[31] G. Szegö, Orthogonal Polynomials, in: Colloquium Publications, Vol. 23 (2003), American Mathematical Society, Providence, Rhode Island, 1939.
[32] C. Miehe, Numerical computation of algorithmic (consistent) tangent moduli in large-strain computational inelasticity, Comput. Methods Appl. Mech. Engrg. 134 (3) (1996) 223–240, http://dx.doi.org/10.1016/0045-7825(96)01019-5.
[33] A. Pérez-Foguet, A. Rodríguez-Ferran, A. Huerta, Numerical differentiation for local and global tangent operators in computational plasticity, Comput. Methods Appl. Mech. Engrg. 189 (1) (2000) 277–296, http://dx.doi.org/10.1016/S0045-7825(99)00296-0.
[34] A. Gizzi, A. Pandolfi, M. Vasta, Statistical characterization of the anisotropic strain energy in soft materials with distributed fibers, Mech. Mater. 92 (2016) 119–138, http://dx.doi.org/10.1016/j.mechmat.2015.09.008.
[35] A. Gizzi, A. Pandolfi, M. Vasta, A generalized statistical approach for modeling fiber-reinforced materials, J. Eng. Math. 109 (1) (2018) 211–226, http://dx.doi.org/10.1007/s10665-017-9943-5.
[36] M. Itskov, A.E. Ehret, R. Dargazany, A full-network rubber elasticity model based on analytical integration, Math. Mech. Solids 15 (6) (2010) 655–671, http://dx.doi.org/10.1177/1081286509106441.
[37] K. Hashlamoun, A. Grillo, S. Federico, Efficient evaluation of the material response of tissues reinforced by statistically oriented fibres, Z. Angew. Math. Phys. 67 (5) (2016) 113, http://dx.doi.org/10.1007/s00033-016-0704-5.
[38] K.-I. Kanatani, Stereological determination of structural anisotropy, Internat. J. Engrg. Sci. 22 (5) (1984) 531–546, http://dx.doi.org/10.1016/0020-7225(84)90055-7.
[39] K. Hashlamoun, S. Federico, Transversely isotropic higher-order averaged structure tensors, Z. Angew. Math. Phys. 68 (4) (2017) 88, http://dx.doi.org/10.1007/s00033-017-0830-8.
[40] G.A. Holzapfel, T.C. Gasser, R.W. Ogden, A new constitutive framework for arterial wall mechanics and a comparative study of material models, J. Elasticity 61 (1) (2000) 1–48, http://dx.doi.org/10.1023/A:1010835316564.
[41] M.B. Rubin, S.R. Bodner, A three-dimensional nonlinear model for dissipative response of soft tissue, Int. J. Solids Struct. 39 (19) (2002) 5081–5099, http://dx.doi.org/10.1016/S0020-7683(02)00237-8.
[42] W. Sun, E.L. Chaikof, M.E. Levenston, Numerical approximation of tangent moduli for finite element implementations of nonlinear hyperelastic material models, J. Biomech. Eng. 130 (6) (2008) 061003, http://dx.doi.org/10.1115/1.2979872.
[43] V. Alastrué, M.A. Martínez, M. Doblaré, A. Menzel, Anisotropic micro-sphere-based finite elasticity applied to blood vessel modelling, J. Mech. Phys. Solids 57 (1) (2009) 178–203, http://dx.doi.org/10.1016/j.jmps.2008.09.005.
[44] F.C. Caner, I. Carol, Microplane constitutive model and computational framework for blood vessel tissue, J. Biomech. Eng. 128 (3) (2006) 419–427, http://dx.doi.org/10.1115/1.2187036.
[45] F.C. Caner, Z. Guo, B. Moran, Z.P. Bažant, I. Carol, Hyperelastic anisotropic microplane constitutive model for annulus fibrosus, J. Biomech. Eng. 129 (5) (2007) 632–641, http://dx.doi.org/10.1115/1.2768378.
[46] G.S. Kassab, M.S. Sacks (Eds.), Structure-Based Mechanics of Tissues and Organs, Springer US, Boston, MA, 2016, http://dx.doi.org/10.1007/978-1-4899-7630-7.

[47] D.H. Cortes, D.M. Elliott, Accurate prediction of stress in fibers with distributed orientations using generalized high-order structure tensors, Mech. Mater. 75 (2014) 73–83, http://dx.doi.org/10.1016/j.mechmat.2014.04.006.
[48] M.S. Abdel-Ghani, G.A. Davies, Simulation of non-woven fibre mats and the application to coalescers, Chem. Eng. Sci. 40 (1) (1985) 117–129, http://dx.doi.org/10.1016/0009-2509(85)85052-1.
[49] T.C. Gasser, R.W. Ogden, G.A. Holzapfel, Hyperelastic modelling of arterial layers with distributed collagen fibre orientations, J. R. Soc. Interface 3 (6) (2006) 15–35, http://dx.doi.org/10.1098/rsif.2005.0073.
[50] S. Federico, T.C. Gasser, Nonlinear elasticity of biological tissues with statistical fibre orientation, J. R. Soc. Interface 7 (47) (2010) 955–966, http://dx.doi.org/10.1098/rsif.2009.0502.
[51] A. Tomic, A. Grillo, S. Federico, Poroelastic materials reinforced by statistically oriented fibres–Numerical implementation and application to articular cartilage, IMA J. Appl. Math. 79 (5) (2014) 1027–1059, http://dx.doi.org/10.1093/imamat/hxu039.
[52] A.E. Ehret, K. Bircher, A. Stracuzzi, V. Marina, M. Zündel, E. Mazza, Inverse poroelasticity as a fundamental mechanism in biomechanics and mechanobiology, Nature Commun. 8 (1) (2017) 1002, http://dx.doi.org/10.1038/s41467-017-00801-3.
[53] A. Stracuzzi, B.R. Britt, E. Mazza, A.E. Ehret, Risky interpretations across the length scales: Continuum vs. discrete models for soft tissue mechanobiology, Biomech. Model. Mechanobiol. 21 (2) (2022) 433–454, http://dx.doi.org/10.1007/s10237-021-01543-4.
[54] K. Bircher, M. Zündel, M. Pensalfini, A.E. Ehret, E. Mazza, Tear resistance of soft collagenous tissues, Nature Commun. 10 (2019) http://dx.doi.org/10.1038/s41467-019-08723-y.
[55] P.J. Blatz, On the thermostatic behavior of elastomers, in: A.J. Chompff, S. Newman (Eds.), Polymer Networks: Structure and Mechanical Properties, Springer US, Boston, MA, 1971, pp. 23–45, http://dx.doi.org/10.1007/978-1-4757-6210-5_2.
[56] G.A. Holzapfel, Nonlinear Solid Mechanics: A Continuum Approach for Engineering, Wiley, 2000.
[57] W. Buerzle, E. Mazza, On the deformation behavior of human amnion, J. Biomech. 46 (11) (2013) 1777–1783, http://dx.doi.org/10.1016/j.jbiomech.2013.05.018.
[58] A. Mauri, A.E. Ehret, D.S.A. De Focatiis, E. Mazza, A model for the compressible, viscoelastic behavior of human amnion addressing tissue variability through a single parameter, Biomech. Model. Mechanobiol. 15 (4) (2016) 1005–1017, http://dx.doi.org/10.1007/s10237-015-0739-0.
[59] B.R. Britt, Supplementary Material: Univariate Gauss Quadrature for Structural Modelling of Tissues and Materials with Distributed Fibres. ETH Research Collection (2023), http://dx.doi.org/10.3929/ethz-b-000620418.
[60] ABAQUS, User Subroutines Reference Guide (6.14), Dassault Systemes Simulia, Inc., 2014.
[61] A.V. Melnik, H. Borja Da Rocha, A. Goriely, On the modeling of fiber dispersion in fiber-reinforced elastic materials, Int. J. Non-Linear Mech. 75 (2015) 92–106, http://dx.doi.org/10.1016/j.ijnonlinmec.2014.10.006.
[62] M. Latorre, F.J. Montáns, On the tension-compression switch of the Gasser–Ogden–Holzapfel model: Analysis and a new pre-integrated proposal, J. Mech. Behav. Biomed. Mater. 57 (2016) 175–189, http://dx.doi.org/10.1016/j.jmbbm.2015.11.018.
[63] C.O. Horgan, J.G. Murphy, On the tension-compression switch hypothesis in arterial mechanics, J. Mech. Behav. Biomed. Mater. 103 (2020) 103558, http://dx.doi.org/10.1016/j.jmbbm.2019.103558.
[64] V. Alastrué, M.A. Martínez, A. Menzel, M. Doblaré, On the use of non-linear transformations for the evaluation of anisotropic rotationally symmetric directional integrals. Application to the stress analysis in fibred soft tissues, Internat. J. Numer. Methods Engrg. 79 (4) (2009) 474–504, http://dx.doi.org/10.1002/nme.2577.
[65] M. Itskov, On the accuracy of numerical integration over the unit sphere applied to full network models, Comput. Mech. 57 (5) (2016) 859–865, http://dx.doi.org/10.1007/s00466-016-1265-3.
[66] E. Verron, Questioning numerical integration methods for microsphere (and microplane) constitutive equations, Mech. Mater. 89 (2015) 216–228, http://dx.doi.org/10.1016/j.mechmat.2015.06.013.
[67] E. Verron, A. Gros, Derivation of full-network models with chain length distribution, in: A. Lion, M. Johlitz (Eds.), Constitutive Models For Rubber X, CRC Press, London, 2017, pp. 587–592, http://dx.doi.org/10.1201/9781315223278-104.
[68] T. Waffenschmidt, A. Menzel, Application of an anisotropic growth and remodelling formulation to computational structural design, Mech. Res. Commun. 42 (2012) 77–86, http://dx.doi.org/10.1016/j.mechrescom.2011.12.004.
[69] A. Menzel, T. Waffenschmidt, A microsphere-based remodelling formulation for anisotropic biological tissues, Phil. Trans. R. Soc. A 367 (1902) (2009) 3499–3523, http://dx.doi.org/10.1098/rsta.2009.0103.